Article

Evidence of human occupation in Mexico around the Last Glacial Maximum

https://doi.org/10.1038/s41586-020-2509-0

Received: 31 August 2018

Accepted: 16 June 2020

Published online: 22 July 2020

Check for updates

Ciprian F. Ardelean[1,2]✉, Lorena Becerra-Valdivia[3,4], Mikkel Winther Pedersen[5], Jean-Luc Schwenninger[3], Charles G. Oviatt[6], Juan I. Macías-Quintero[7], Joaquin Arroyo-Cabrales[8], Martin Sikora[5], Yam Zul E. Ocampo-Díaz[9,10], Igor I. Rubio-Cisneros[10], Jennifer G. Watling[11], Vanda B. de Medeiros[12], Paulo E. De Oliveira[12,13], Luis Barba-Pingarón[14], Agustín Ortiz-Butrón[14], Jorge Blancas-Vázquez[14], Irán Rivera-González[15], Corina Solís-Rosales[16], María Rodríguez-Ceja[16], Devlin A. Gandy[17], Zamara Navarro-Gutierrez[1], Jesús J. De La Rosa-Díaz[1], Vladimir Huerta-Arellano[1], Marco B. Marroquín-Fernández[7], L. Martin Martínez-Riojas[1], Alejandro López-Jiménez[8], Thomas Higham[3] & Eske Willerslev[5,18,19,20]✉

The initial colonization of the Americas remains a highly debated topic[1], and the exact timing of the first arrivals is unknown. The earliest archaeological record of Mexico—which holds a key geographical position in the Americas—is poorly known and understudied. Historically, the region has remained on the periphery of research focused on the first American populations[2]. However, recent investigations provide reliable evidence of a human presence in the northwest region of Mexico[3,4], the Chiapas Highlands[5], Central Mexico[6] and the Caribbean coast[7–9] during the Late Pleistocene and Early Holocene epochs. Here we present results of recent excavations at Chiquihuite Cave—a high-altitude site in central-northern Mexico—that corroborate previous findings in the Americas[10–17]of cultural evidence that dates to the Last Glacial Maximum (26,500–19,000 years ago)[18], and which push back dates for human dispersal to the region possibly as early as 33,000–31,000 years ago. The site yielded about 1,900 stone artefacts within a 3-m-deep stratified sequence, revealing a previously unknown lithic industry that underwent only minor changes over millennia. More than 50 radiocarbon and luminescence dates provide chronological control, and genetic, palaeoenvironmental and chemical data document the changing environments in which the occupants lived. Our results provide new evidence for the antiquity of humans in the Americas, illustrate the cultural diversity of the earliest dispersal groups (which predate those of the Clovis culture) and open new directions of research.

The archaeological site of Chiquihuite Cave is located in the Astillero Mountains, Zacatecas, at 2,740 m above mean sea level and about 1,000 m above the valley floor (Extended Data Fig. 1a–c). The cave was formed by dissolution and the roof collapse of nearly vertical (dip overturned; 80° southwest, strike 320°) Jurassic limestone, deformed during the Laramide orogeny of the Late Cretaceous and early Palaeogene periods. It has 2 interconnecting chambers, each of which is more than 50 m wide and about 15 m high, and contains speleothems (Fig. 1a). The inclined floor has accumulated roof-fall blocks and debris flow deposits that entered through the mouth of the cave, sealing it by the terminal Pleistocene epoch (Extended Data Fig. 1d, e, h). The cave is currently active, with continued speleothem growth and water drip that intensifies during the rainy season.

In 2012, materials found in a first test pit (excavation designated X-11) inside the main chamber suggested a human presence dating to or before the Last Glacial Maximum (LGM)[2,19] (between about 26,000

[1]Unidad Académica de Antropología, Universidad Autónoma de Zacatecas, Zacatecas, Mexico. [2]Department of Archaeology, University of Exeter, Exeter, UK. [3]Research Laboratory for Archaeology and History of Art, University of Oxford, Oxford, UK. [4]Chronos 14C-Cycle Facility, SSEAU, University of New South Wales, Sydney, New South Wales, Australia. [5]Lundbeck Foundation GeoGenetics Centre, University of Copenhagen, Copenhagen, Denmark. [6]Department of Geology, Kansas State University, Manhattan, KS, USA. [7]Escuela de Arqueología, Universidad de Ciencias y Artes de Chiapas, Tuxtla Gutiérrez, Mexico. [8]Laboratorio de Arqueozoología, Subdirección de Laboratorios y Apoyo Académico, Instituto Nacional de Antropología e Historia, Mexico City, Mexico. [9]Facultad de Ingeniería, Universidad Autónoma de San Luís Potosí, San Luis Potosí, Mexico. [10]Grupo de Geología Exógena y del Sedimentario, San Luis Potosí, Mexico. [11]Laboratório de Arqueologia dos Trópicos, Museu de Arqueologia e Etnologia, Universidade de São Paulo, São Paulo, Brazil. [12]Laboratório de Micropaleontologia, Instituto de Geociências, Universidade de São Paulo, São Paulo, Brazil. [13]Botany Department, The Field Museum of Natural History, Chicago, IL, USA. [14]Laboratorio de Prospección Arqueológica, Instituto de Investigaciones Antropológicas (IIA), Universidad Nacional Autónoma de México (UNAM), Mexico City, Mexico. [15]Laboratorio de Palinología, Escuela Nacional de Antropología e Historia (ENAH), Mexico City, Mexico. [16]Laboratorio de Espectrometría de Masas con Aceleradores, Instituto de Física, Universidad Nacional Autónoma de México (UNAM), Mexico City, Mexico. [17]Department of Archaeology, University of Cambridge, Cambridge, UK. [18]Welcome Trust, Sanger Institute, Hinxton, UK. [19]The Danish Institute for Advanced Study, University of Southern Denmark, Odense, Denmark. [20]Department of Zoology, University of Cambridge, Cambridge, UK. ✉e-mail: aeci000206@uaz.edu.mx; ewillerslev@sund.ku.dk

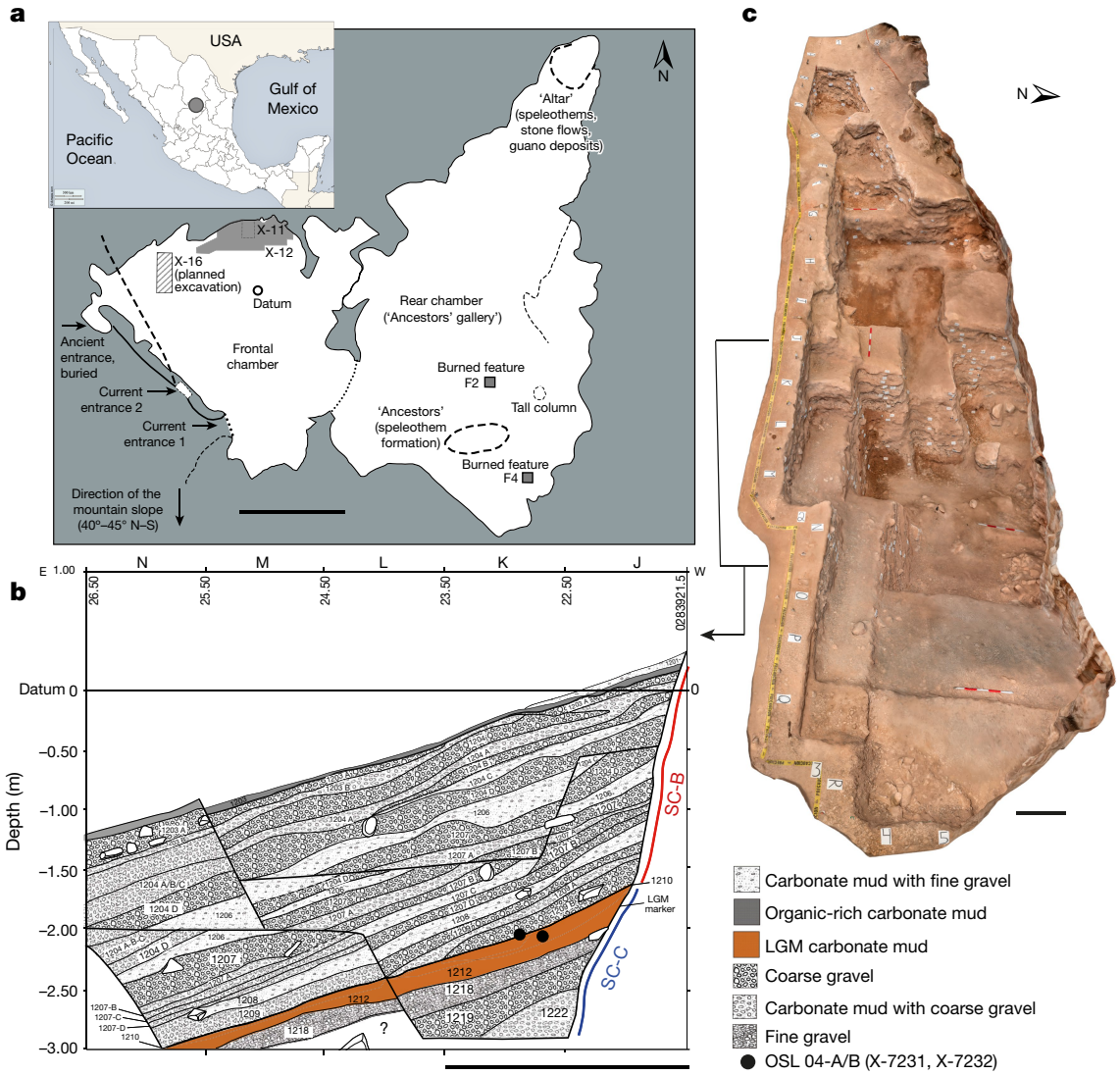

Fig. 1 | Setting of Chiquihuite Cave, and the X-12 excavation. a, Planimetry of the cave; X-12 is along the northern wall of the main chamber. Scale bar, 20 m. The inset situates the site in Mexico; free map downloaded from www.d-maps.com. **b**, **c**, Drawing of the type (southern) stratigraphic profile of the central-eastern sectors of X-12 (**b**), corresponding to the area indicated on the semi-vertical view of the 3D photogrammetric model of the excavation (**c**). Scale bars, 2 m (**b**) and 1 m (**c**). Numbers along the *x* axis (grid squares) in **b** refer to UTM (Universal Transverse Mercator) coordinates. More detailed information is provided in Extended Data Figs. 1, 2, 7. All photographs are of our authorship.

and 18,000–19,000 years ago[18]). To investigate this further, the original unit was enlarged through a more extensive excavation (designated X-12) in 2016–2017. The excavation area—located 50 m inwards from the current entrance of the cave—was free of roof-collapse boulders on its surface and was partially sealed under flowstone (in its western half; squares A–I) (Fig. 1c, Extended Data Fig. 1i). The excavation covered 62 m^2 (a maximum extent of 18 × 5 m) and had a maximum depth of 3 m, stepping down gradually from both ends towards the deepest layers in the central-eastern sector (squares J–M) (Extended Data Figs. 1h, i, 2). Stratified sediments were traced along the trench and correlated on profiles (Extended Data Fig. 7). Beds were roughly parallel, dipping at 25° E and thickening as the slope decreased the same direction.

Strata contain mainly angular grey limestone fragments that range in size from granules to boulders. The gravels are coated with fine-grained carbonate sediment that, in places, fills pore spaces and appears 'muddy' relative to the larger particles of limestone gravel (Supplementary Information 1.1.3). This gives an appearance of alternating gravel and muddy layers. On north–south profiles, the gravel units appear as tilted lenses or wedges. On the south profile, these units have a more uniform thickness (Fig. 1b, Extended Data Figs. 2, 7). The basal contacts of the coarse units are abrupt, whereas their upper contacts are transitional to the overlying muddy units (Extended Data Fig. 1f, g). We interpreted the coarse sediments as alluvial and colluvial debris flows that were generated outside and deposited inside the cave, and the finer-grained muddy sediments as derived from wind-blown dust and the impacts of roof-fall blocks. The influx rate of wind-blown dust was probably greater during drier phases in the Late Pleistocene. We found no evidence of animal burrowing or other stratigraphic disturbances. The inclination of the deposits would have allowed the horizontal displacement of archaeological materials along individual strata. Substantial vertical movement is unlikely, given the tight gravel beds and underlying muddy units.

Stratum 1212—which is relatively thick, and has a distinctive orange and brown colour (suggestive of a moderate state of oxidation)—was used as a chronostratigraphic marker to divide the deposits into two stratigraphic components (designated SC-B and SC-C; SC-A refers to the current cave floor, incorporating modern and historical site use) (Fig. 1b, Extended Data Fig. 2, Supplementary Information 4).

The overlying coarse layers were easily separable while digging, exposing a smooth upper contact (stratum 1210). Stratum 1210 was hardened and compacted, either intentionally or as a result of repeated stepping. The geomorphology of this surface reveals prolonged exposure before burial (Supplementary Information 1.7.1). We interpret strata 1212 and 1210 as having formed in a drier, more-stable climate during or at the end of the LGM, when debris flows were not as common as the periods before and after it. SC-C thus comprises the terminal LGM and preceding depositional events.

Chronology

We obtained 46 radiocarbon determinations from a total of 59 samples (bone, charcoal and sediment), as well as 6 optically stimulated luminescence (OSL) dates from a total of 8 samples (Extended Data Table 1, Supplementary Information 1.2, 1.8, 1.9). The chronology at Chiquihuite Cave is principally constructed using radiocarbon dating, with OSL dates providing an independent control. Sample selection was aimed at maintaining a close spatial relationship with lithic artefacts found along the sequence (Extended Data Fig. 3, Supplementary Video 1). All bone samples—except for LEMA-640.1.1 (LEMA, Laboratorio de Espectrometría de Masas con Aceleradores)—with reported elemental and isotopic data ($n = 6$) had collagen yields, C:N atomic ratios and per cent carbon values that fell within accepted ranges (greater than 1% (weight), 2.9–3.5 and 30–50% (weight), respectively[20]). This indicated acceptable collagen preservation and likely low levels of contamination.

All the chronometric data we obtained (Extended Data Table 1) were incorporated into a Bayesian age model (Fig. 2, Supplementary Information 1.2) with the exception of LEMA-977, a bone from stratum 1201 (in SC-A) of historical date; LEMA-640.1.1, which failed collagen quality-control values set by Oxford Radiocarbon Accelerator Unit[20] (ORAU; samples designated by OxA- numbers); and the bulk sediment dates (LEMA 575.1.2, Beta 436709 and International Chemical Analysis (ICA)-16OS/0510), as these often yield minimum ages owing to low amounts of carbon and the potential for contamination[21,22]. Modelled output estimates the start of SC-C as being before the LGM, at 33,150–31,405 calibrated years before present (AD 1950) (cal. BP) (all ranges are given at 95.4% probability); SC-B dates to between 16,605–15,615 cal. BP and 13,705–12,200 cal. BP (close in date to the Younger Dryas, at about 12,900–11,700 years ago[23]). The entire sequence spans 20,090–17,830 years. Five dates—LEMA-577.1.1, LEMA-576.1.1, OxA-36613, OxA-36359 and LEMA-978.1.1—were identified as major outliers by the outlier model we applied (Fig. 2). These inconsistencies might be due to taphonomic factors or incomplete decontamination. All outliers are down-weighted in the model in proportion to their measured outlier probability. Within the sequence, we identified a considerable gap between strata 1218–1219 and stratum 1217 that fits within the LGM, and probably indicates decreased human presence and reduced sedimentation. Overall, the chronological sequence for Chiquihuite Cave is in excellent agreement with the stratigraphic evidence.

Stone tool assemblage

Stone tools ($n = 1{,}930$) were found in all excavated strata, at a higher frequency in SC-B than SC-C (Fig. 3, Extended Data Figs. 5, 6, Supplementary Information 1.3). SC-B yielded 87.2% of the assemblage ($n = 1{,}684$); only 12.3% ($n = 239$) of the tools were recovered from underlying SC-C (Fig. 1b). The comparatively low number of artefacts in SC-C is probably biased by the smaller volume of excavated sediment for this component. However, their presence provides evidence for cultural activity in the lowermost strata, where vertical displacement is unlikely. Such a taphonomic phenomenon is even less probable for cultural items found in older strata, deeply buried underneath the base of SC-B—for example, a bifacial lanceolate perform (Fig. 3m) excavated from stratum 1223, 1.1 m below stratum 1212.

The flaked artefacts reflect a technological tradition that was previously unknown, and remains mostly unchanged over the sequence. The interpretation of specific variations in the technological and typological parameters is limited by the excavation-volume bias. Despite an expedient aspect, the assemblage reveals advanced flaking skills applied to a challenging raw material, consistently represented by green and blackish varieties of recrystallized limestone (mudstone–wackestones of pellets[24], or pelsparite–pelmicrite[25]). Unlike the grey gravels found inside the cave and on the outside slope, these finer-grained stone varieties are moderately recrystallized and have good isotropy (similar to any chert), and are suitable for controlled flaking (Supplementary Information 1.7). The lithic artefacts were made almost exclusively (>90%) from the green or blackish varieties, which reveals intentional selectivity. Although rare, the green or black limestones are available in the vicinity of the site, in the form of small loose nodules that have eroded from as-yet unidentified geological sources. Results from thin-section petrographic analyses suggest that these particular limestones do not belong to the petrology of the cave, being morphologically different from the rock conforming the walls and roof as well as from the dominant grey clastic material (Supplementary Information 1.7, Supplementary Fig. 28). The systematic geological selectivity observed in the manufacture of stone tools probably reflects conscious decision-making and an intimate knowledge of the available stone stock. However, a few cortical and secondary flakes of grey limestone are found—probably as a result of the testing of stone nodules during material selection. The use of silica-rich limestones for tool-making is widespread in other Pleistocene–Holocene archaeological sites across the study region[19].

Tools were manufactured principally on previously extracted (mainly transversal) flakes and small tabular and irregular nodules (3–7 cm in maximum dimension) reduced by bifacial and unifacial approaches. This particular raw material (blanks of a small size) favours the extraction of transversal flakes when nonpunctual, flat, wide or dihedral striking platforms are used. The dominant technique is direct percussion, with pressure-flaking occasionally (and exclusively) used for platform isolation. Flakes were shaped into tools by marginal retouch, through percussion trimming. A preliminary morpho-technological typology includes cores, flakes, blades, bladelets, modified or used flaking debris (debitage), scrapers, points, adzes and point-like items shaped by fracturing the edges of limestone and calcite laminae.

The debitage (66% of the total) includes primary, secondary and tertiary flakes (Fig. 3b–e, Extended Data Fig. 5f–n). The repeated failed blows and error repairs are another reliable indicator of intentionality, expert guidance and learning—as is the presence of supernumerary platforms on some of the flakes. Flake platforms are prepared (dihedral, faceted, and isolated), punctiform (often ground) or left flat and wide, tilted towards the ventral face (Fig. 3b–d, Extended Data Figs. 5n, p, q, s, 6c). Many platforms are lipped, which suggests the use of soft hammers (of antler, bone or hardwood) (Fig. 3c, d, Extended Data Fig. 5j, k). Over-prepared platforms were strengthened by edge grinding, then micro-flaked as faceted or isolated spots meant for well-controlled impact. The flakes that follow a ridge and cortical starter flakes lack platform preparation. The apparent technological signature of this industry is the transversal point, which is well-represented in the assemblage. Such points are obtained by the marginal retouch (edge trimming) of transversal flakes, the platforms of which are set aside, and the direction of extraction is perpendicular to the long axis (Extended Data Figs. 5j–l, 6n, o, s–z, a′, d′, e′, f′, g′). The frequency of overshot (*outrepassé*) flakes is explained by the small size of the blanks. Blade production is represented at the site by corner blades with unprepared platforms, but also by true, curved, prismatic functional blades (Fig. 3f–j, Extended Data Figs. 5o–x, 6d–i). The abundance of bladelets and blade medial fragments (obtained by fracturing larger blades), with used edges, suggests a microlithic technology (Fig. 3i, Extended Data Figs. 5u–x, 6d, e).

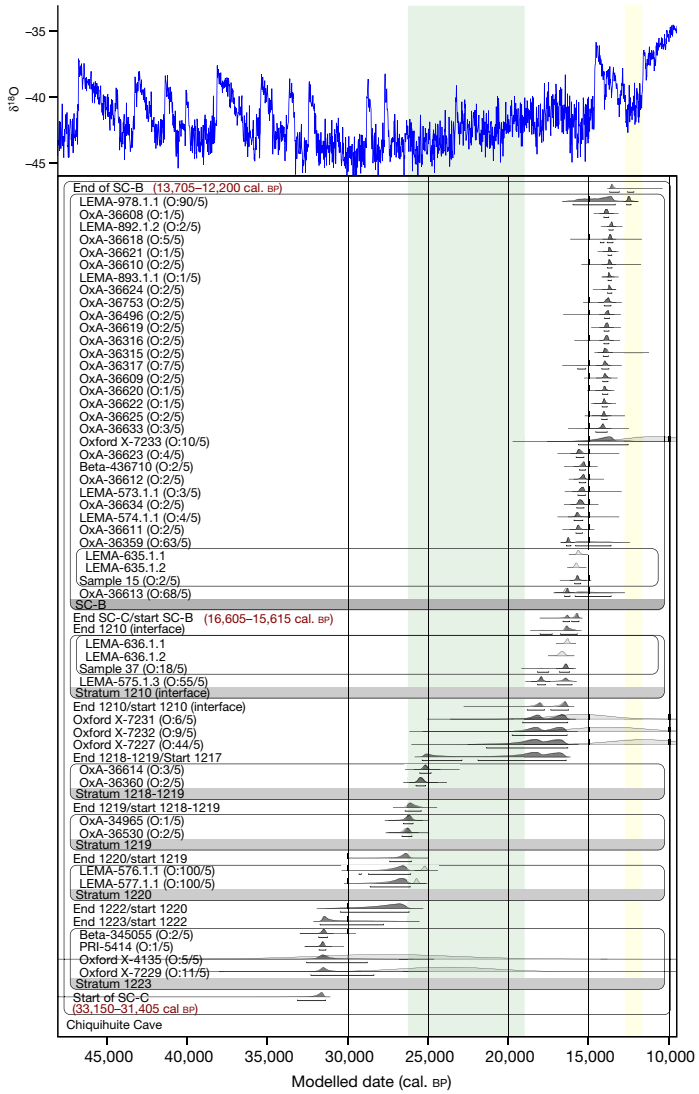

Fig. 2 | Bayesian age model of Chiquihuite Cave. The green band represents the span of the LGM (per ref. [18]) and the yellow indicates the Younger Dryas (per ref. [21]). C, convergence values. Outlier analysis output (O) is noted as 'posterior probability/prior probability'. Outliers are down-weighted according to the posterior outlier probability, so a date with 100% outlier probability does not contribute to the posterior distributions. $\delta^{18}O$ data according to the Greenland ice core timescale (GICC05)[35]. Modelled output estimates the start of SC-C to 33,150–31,405 cal. BP (pre-LGM) (all ranges are given at 95.4% probability and noted in red), with the commencement of SC-B at 16,605–15,615 cal. BP and its end at 13,705–12,200 cal. BP. Further information on chronometric data is provided in Extended Data Table 1.

The assemblage contains modified or used debitage, which often manifests as use-wear damage on sharp edges (26.8%). A frequent approach is the shaping of flakes and laminae into circular, square or polygonal objects, by snapping and abrupt flaking (which is also seen in points) (Extended Data Fig. 5n, b′, c′, e′, m′, n′ o′, p′, q′). Burins (Extended Data Fig. 5y, w) and small backed knives are also present. Thick flakes and nodules often became edge-modified tools. Circular scrapers and endscrapers show steep retouch on robust flakes (Extended Data Figs. 5z, a′, 6j). The square-edge management—an important indicator of human reasoning and intentionality—appears when natural square edges are systematically reduced by bifacial alternating flaking (Fig. 3n).

Points and point-like shapes are frequent and varied (forming 31% of the total assemblage) (Fig. 3k–o). However, the majority of these tools are unifacial with marginal retouch (for example, the transversal points) (Extended Data Figs. 5a, c, e–m, 6n, o, s–z, a′, d′, e′, f′, g′). Others are proper bifaces, made on flakes or nodules (Fig. 3k–m). Apart from incipient preforms, finished bifacial artefacts are scarce; their existence is inferred from the abundance of tertiary thinning flakes. Notches and stems are almost completely absent. The bases are rounded or convergent, and are rarely thinned. Among cores ($n = 30$), the type that we designated 'b' is of special interest. It is bifacial, biconvex, has dorsal–ventral symmetry and alternating flaking around its medial edge, apparently prepared for the extraction of a single flake from one face (Fig. 3a, Extended Data Figs. 5b, 6a).

The recurrent techno-morphological combinations in the assemblage reveal evident intentionality and systematization in the creation of human-made artefacts, as well as evident standardization at the level of individual pieces. Overall, the assemblage represents a lithic industry with no evident similarities to any of the other cultural complexes of the Pleistocene or Early Holocene epochs known in the Americas[26–28].

Palaeoenvironment and environmental DNA

We performed 31 DNA extractions on samples from 15 key stratigraphic units (including controls), and tested for the presence of ancient environmental DNA[29] (Extended Data Fig. 2, Supplementary Information 4, Supplementary Data). Initially, we evaluated the efficiency of two lysis buffers to yield DNA (Supplementary Information 1.10). All samples

Fig. 3 | Examples of lithic artefacts from Chiquihuite Cave. a, Core. **b**–**e**, Flakes; inlay in **b** emphasizes an isolated platform. **f**–**j**, Blades. **k**–**o**, Points. Scale bar, 3 cm. Most items are from component SC-B; **d** and **m** belong to SC-C. One *Pseudotsuga* sp. (Douglas fir) charcoal fragment closely associated with the bifacial preform shown in **m** in stratum 1223 was dated to 27,929 ± 82 uncalibrated radiocarbon years BP (PRI-5414). More lithic finds are shown in Extended Data Figs. 5, 6.

were then converted into 37 Illumina libraries and shotgun-sequenced for a preliminary reconstruction of past organismal assemblages (Extended Data Fig. 4). Taxonomic identification of all sequenced reads followed the latest protocols, designed to avoid false positives and to perform robust taxonomic identification[30]. We also tested the specificity and sensitivity of our assignment method using comprehensive in silico modelling, simulating damage, and sequenced fragmented DNA for key taxa found in the samples (Supplementary Information 1.10).

During the pre-LGM to terminal-LGM period (strata 1223–1210), ancient environmental DNA shows the presence of mixed forest species—junipers (*Juniperus*), firs (*Abies*), pine (*Pinus*) and spruce (*Picea*)—complemented by grasses (*Lolium* sp., Pooideae and *Hordeum*), rosids and *Castilleja* sp. (Extended Data Fig. 4, Supplementary Information 1.10, Supplementary Figs. 54, 55). The pre-LGM and LGM (strata 1223–1212) were more forested than later periods, and showed the highest abundances of trees and forbs (such as *Castilleja* sp.). A clearer shift in the plant community occurs after the LGM but before the Younger Dryas (strata 1207A and 1204). In this shift, pines and juniper nearly disappear, and the DNA record becomes dominated by Agavoideae (probably Joshua trees (*Yucca* spp.)), the pine subgroup *Strobus* and *Aegilops*, and *Sorghum* and grasses within the Tripsacinae family and PACMAD clade (Panicoideae, Arundinoideae, Chloridoideae, Micrairoideae, Aristidoideae and Danthonioideae), which replace the previous grass species (*Lolium, Hordeum* and Pooideae).

We also performed phytolith and pollen analyses; some of the plant taxa we identified are similar to those in the environmental DNA results, and others differ (Supplementary Information 1.6). As with environmental DNA, evidence from phytolith and pollen proxies supports a rapid transition to colder conditions in the LGM, and the presence of a relatively open environment dominated by cold-adapted grasses. The presence of palm (Arecaceae) phytoliths in all samples—including those constrained to the LGM—deserves attention, and replicates the discovery of similar burnt specimens in X-11[2,19]. This is because at present only one (*Brahea berliandieri*) of the five palm species native to Zacatecas[31] grows on the local mountain slopes (below 2,000 m above mean sea level)[32]. These phytoliths could have entered the cave naturally if *Brahea* grew at higher altitudes during warmer climatic phases; however, climatic conditions during the LGM were colder than the present. It is therefore a possibility that these were brought into the cave by humans in the form of perishable artefacts or food. The burnt condition of some of the phytoliths supports this hypothesis. All strata yielded charcoal fragments (≥1 cm) and mesocharcoals (180–1,000 µm)—probably the result of a combination of wildfires outside, and human-made fireplaces located at the entrance of, the cave.

Among the fauna, bat DNA is present in all layers. This is dominated by *Eptesicus* sp., *Myotis* sp. and Vespertilionidae, until stratum 1204, in which Phyllostomidae, *Desmodus* sp. and new Microchiroptera species replace the previous assemblage. By contrast, although bear DNA (*Ursus* sp.) appears during the LGM, the highest abundance occurs during the termini, which is in concordance with the archaeological evidence[2,19] (Supplementary Information 1.5, Supplementary Fig. 7). Rodents (*Marmota* sp., *Microtus* sp., *Ictidomys* sp., *Urocitellus* sp. and *Peromyscus* sp.) are present throughout the sequence, with a higher incidence in a few of the strata. Deer mouse (*Peromyscus* sp.), vole (*Microtus* sp.) and marmot (*Marmota* sp.) appear to be more abundant than other rodents, with kangaroo rat (*Dipodomys* sp.) appearing in the youngest stratum (stratum 1201). DNA findings also include goat (Caprinae, probably *Oreamnos* sp.) and sheep (*Ovis* sp.), as well as a low proportion of DNA from birds, such as sparrow (*Zonotrichia* sp.), falcon (*Falco* sp.) and tanagers (Thraupidae).

We also attempted to identify ancient human DNA (*Homo* sp.) from all layers. Our analyses focused on strata with longer occupational contexts (strata 1204, 1210, 1212 and 1218), for which additional extraction, libraries and sequencing efforts were performed (Supplementary Information 1.10, Supplementary Data). However, we found no evidence of ancient human DNA within the samples. This does not negate a human presence at Chiquihuite Cave, as the probability of detecting ancient human DNA from cave sediments has previously been shown to be low[33].

To assess the degree of DNA leaching, we tested for the presence of recent horse (*Equus*) DNA in all layers. This genus was selected because a

horse enclosure was historically located on top of the excavated layers, in the northeastern corner of the main chamber. Results found modern horse DNA to be present in the uppermost stratum (stratum 1201, with most reads aligning to donkey, *Equus asinus*), and ancient horse DNA in the seven strata below (strata 1204C, 1207C, 1208, 1215, 1217, 1218, and 1223)—with more reads aligning to the last-surviving wild horse (*Equus przewalskii*) than to *E. asinus* (Supplementary Information 2, Supplementary Data), and with DNA damage similar to the levels found in the remainder of the faunal record. Therefore, DNA leaching is not considered a factor.

Within the faunal bone assemblage we extracted (n = 1,850), microfauna (Cricetidae, 38%; Chiroptera, 25%; as well as Leporidae and Aves) is the most abundant (Supplementary Information 1.5). The LGM strata mark the appearance of larger genera—black bear (*Ursus americanus*), condor (*Gymnogyps* sp.), otter (*Lontra* sp.)—that are absent from the bone assemblage of upper layers. Snails replicate modern taxa (Urocoptidae (56%) and *Humboldtiana* sp. (43%)), which are fit for rocky forest soils (Supplementary Information 1.5, Supplementary Fig. 7).

Adding to the environmental DNA data, chemical residues from the interface of 1210 (terminal- to post-LGM) revealed high concentrations of proteins, phosphates, carbohydrates and fatty acids (Supplementary Information 1.4). As these are unlikely to be the product of natural limestone decay, such enrichment may relate to human or faunal activities. An analysis of the spatial distribution of X-ray fluorescence values for sulfur, potassium and zinc—elements that we interpret as derivatives of human activities—match the distributions of chemical residues. The relationship between phosphates and zinc, which has previously been recognized as an indicator of refuse areas[34], is also evident in this stratum. Potassium concentrations probably indicate the accumulation of ash from cellulosic fuels, and sulfur (which is present in living cells) follows similar X-ray fluorescence and chemical-residue distribution patterns.

Conclusion

Stone tools and chemical residue evidence suggest that humans were present in Chiquihuite Cave, at least between the LGM terminus and the onset of the Younger Dryas. LGM and pre-LGM human presence is supported by stone flaked artefacts in SC-C, below stratum 1212. Cultural evidence for this phase is comparatively scarce (possibly reflecting shorter and infrequent visits), but still suggests a much earlier human arrival on the continent than previously appreciated. Given the length of the sequence at Chiquihuite, it is likely that humans used the site on a relatively constant basis, perhaps in recurrent seasonal episodes that were part of larger migratory cycles. The high altitude of the cave makes it an atypical location for human occupation of the Americas in the Pleistocene epoch, breaking the pattern of megafauna kill sites, open sites and shallow rockshelters. The occupants of the cave were seemingly adapted to altitudes and mountain landscapes, showing a behavioural pattern that—to our knowledge—was previously unknown in the archaeological record of the Americas. Their lithic industry has no parallel in the continent and its qualitative traits suggest a mature technology, possibly brought in from elsewhere before the LGM.

Further archaeological and environmental DNA work is required to better elucidate the origins of the inhabitants of Chiquihuite Cave, their bio-cultural relationship to other older-than-Clovis groups and the path that their ancestors followed to the Americas.

Online content

Any methods, additional references, Nature Research reporting summaries, source data, extended data, supplementary information, acknowledgements, peer review information; details of author contributions and competing interests; and statements of data and code availability are available at https://doi.org/10.1038/s41586-020-2509-0.

1. Meltzer, D. J. *The Great Paleolithic War: How Science Forged an Understanding of America's Ice Age Past* (Univ. Chicago Press, 2015).
2. Ardelean, C. F. et al. in *People and Culture in Ice Age Americas: New Dimensions in Paleoamerican Archaeology* (eds Suarez, R. & Ardelean, C. F.) 108–133 (Univ. Utah Press, 2019).
3. Sanchez, G. et al. Human (Clovis)–gomphothere (*Cuvieronius* sp.) association ~13,390 calibrated yBP in Sonora, Mexico. *Proc. Natl Acad. Sci. USA* **111**, 10972–10977 (2014).
4. Des Lauriers, M. R., Davis, L. G., Turnbull, J., Southon, J. R. & Taylor, R. E. The earliest fish hooks from the Americas reveal fishing technology of Pleistocene maritime foragers. *Am. Antiq.* **82**, 498–516 (2017).
5. Acosta, G. et al. Climate change and peopling of the Neotropics during the Pleistocene–Holocene transition. *Bol. Soc. Geol. Mex.* **70**, 1–19 (2018).
6. González, S., Jiménez López, C., Hedges, R., Pompa y Padilla, J. A. & Huddart, D. Early humans in Mexico: new chronological data. In *El Hombre Temprano en América y sus Implicaciones en el Poblamiento de la Cuenca de México: Primer Simposio Internacional* (eds Jiménez López, C. et al.) 67–77 (Instituto Nacional de Anthrología e Historia, 2006).
7. González, A. et al. in *Paleoamerican Odyssey* (eds Graf, K. E. et al.) 323–337 (Center for the Study of the First Americans, 2014).
8. Chatters, J. C. et al. Late Pleistocene human skeleton and mtDNA link Paleoamericans and modern Native Americans. *Science* **344**, 750–754 (2014).
9. Stinnesbeck, W. et al. The earliest settlers of Mesoamerica date back to the late Pleistocene. *PLoS ONE* **12**, e0183345 (2017).
10. Williams, T. J. et al. Evidence of an early projectile point technology in North America at the Gault Site, Texas, USA. *Sci. Adv.* **4**, eaar5954 (2018).
11. Waters, M. R. et al. Pre-Clovis projectile points at the Debra L. Friedkin site, Texas–implications for the Late Pleistocene peopling of the Americas. *Sci. Adv.* **4**, eaat4505 (2018).
12. Jenkins, D. L. et al. Clovis age Western Stemmed projectile points and human coprolites at the Paisley Caves. *Science* **337**, 223–228 (2012).
13. Adovasio, J. M., Gunn, J. D., Donahue, J. & Stuckenrath, R. Meadowcroft Rockshelter, 1977: an overview. *Am. Antiq.* **43**, 632–651 (1978).
14. Halligan, J. J. et al. Pre-Clovis occupation 14,550 years ago at the Page–Ladson site, Florida, and the peopling of the Americas. *Sci. Adv.* **2**, e1600375 (2016).
15. Dillehay, T. D. *Monte Verde, a Late Pleistocene Settlement in Chile: The Archaeological Context and Interpretation* (Smithsonian Institution Press, 1997).
16. Bourgeon, L., Burke, A. & Higham, T. Earliest human presence in North America dated to the Last Glacial Maximum: new radiocarbon dates from Bluefish Caves, Canada. *PLoS ONE* **12**, e0169486 (2017).
17. Davis, L. G. et al. Late Upper Paleolithic occupation at Cooper's Ferry, Idaho, USA, ~16,000 years ago. *Science* **365**, 891–897 (2019).
18. Clark, P. U. et al. The Last Glacial Maximum. *Science* **325**, 710–714 (2009).
19. Ardelean, C. F. *Archaeology of Early Human Occupations and the Pleistocene–Holocene Transition in the Zacatecas Desert, Northern Mexico*. PhD thesis, Univ. Exeter (2013).
20. Brock, F., Higham, T., Ditchfield, P. & Bronk Ramsey, C. Current pretreatment methods for AMS radiocarbon dating at the Oxford Radiocarbon Accelerator Unit (ORAU). *Radiocarbon* **52**, 103–112 (2010).
21. Wang, Y., Amundson, R. & Trumbore, S. Radiocarbon dating of soil organic matter. *Quat. Res.* **45**, 282–288 (1996).
22. Pessenda, L. C. R., Gouveia, S. E. M. & Aravena, R. Radiocarbon dating of total soil organic matter and humin fraction and its comparison with ^{14}C ages of fossil charcoal. *Radiocarbon* **43**, 595–601 (2001).
23. Rasmussen, S. O. et al. A stratigraphic framework for abrupt climatic changes during the Last Glacial period based on three synchronized Greenland ice-core records: refining and extending the INTIMATE event stratigraphy. *Quat. Sci. Rev.* **106**, 14–28 (2014).
24. Dunham, R. J. Classification of carbonate rocks according to depositional texture. In *Classification of Carbonate Rocks—A Symposium* (ed. Ham, W. E.) 108–121 (The American Association of Petroleum Geologists, 1962).
25. Folk, R. L. Practical petrographic classification of limestones. *Bull. Am. Assoc. Petrol. Geol.* **43**, 1–38 (1959).
26. Smallwood, A. M. & Jennings, T. A. *Clovis: On the Edge of a New Understanding* (Texas A&M Univ. Press, 2014).
27. Goebel, T. & Keene, J. L. in *Archaeology in the Great Basin and Southwest: Papers in Honor of Don D. Fowler* (eds Parezo, N. J. & Janetski, J. C.) 35–60 (Univ. Utah Press, 2014).
28. Graf, K. E. & Buvit, I. Human dispersal from Siberia to Beringia: assessing a Beringian standstill in light of the archaeological evidence. *Curr. Anthropol.* **58**, S583–S603 (2017).
29. Willerslev, E. et al. Diverse plant and animal genetic records from Holocene and Pleistocene sediments. *Science* **300**, 791–795 (2003).
30. Pedersen, M. W. et al. Postglacial viability and colonization in North America's ice-free corridor. *Nature* **537**, 45–49 (2016).
31. Villaseñor, J. L. Checklist of the native vascular plants of Mexico. *Rev. Mex. Biodivers.* **87**, 559–902 (2016).
32. Henderson, A., Bernal, R. & Galeano-Garces, G. *Field Guide to the Palms of the Americas* (Princeton Univ. Press, 1997).
33. Slon, V. et al. Neandertal and Denisovan DNA from Pleistocene sediments. *Science* **356**, 605–608 (2017).
34. Middleton, W. D. et al. The study of archaeological floors: methodological proposal for the analysis of anthropogenic residues by spot tests, ICP-OES, and GC-MS. *J. Archaeol. Method Theory* **17**, 183–208 (2010).
35. Rasmussen, S. O. et al. A new Greenland ice core chronology for the last glacial termination. *J. Geophys. Res.* **111**, D06102 (2006).

Methods

No statistical methods were used to predetermine sample size. The experiments were not randomized and investigators were not blinded to allocation during experiments and outcome assessment.

Discovery and fieldwork

This work forms part of the 'Pleistocene Hunters of the Northern Highlands Archaeological Project', which has identified >30 hunter-gatherer sites within the endorheic basin of Concepción del Oro. The discovery of caves was a priority. No computational predictive models were used; only systematic walking, landform interpretation and guidance from locals in Guadalupe Garzarón, the nearest village. C.F.A. and J.I.M.-Q. first visited Chiquihuite Cave on 16 May 2010, and registered the site with the Mexican government: the site register number is G14C6332001/ID 44499. Fieldwork continued with the local permission and official permits from the Archaeology Council of Mexico (Instituto Nacional de Antropología e Historia (INAH)). The two seasons reported here totalled 80 working days, in January–February 2016 and December 2016–January 2017. Because of the location, the crew could not travel daily but lived at the site for the entire season. All supplies and materials were carried from the beginning, in caravans of about 30 villagers with animals. Topography impedes the use of vehicles or helicopters. The crew was limited to 8 members living inside the main chamber—where temperature stabilizes at 12 °C, regardless of the external weather. We used conventional light bulbs and LED reflectors connected to an eco-friendly Honda EU10 power generator.

Excavation

For X-12, strata nomenclature was reformulated, keeping only necessary correlations with X-11. The 1 × 1-m squares were divided in 0.5 × 0.5-m intercardinal subsquares. Their codes combine letters (southern profile) and numbers (S–N axis) (Extended Data Fig. 1i). All finds were referred to squares and subsquares (for example, M4-NW for the northwestern quadrant of square M4). We avoided permanent grids because: (a) anchoring was impossible owing to the height of the ceiling and the concretions on the northern wall, and (b) strings increase the risk of accidents and threaten the integrity of the profiles. We installed a white perimeter string, using a Brunton compass, theodolite and trigonometry. Wooden or metal pegs and string marks at each metre were tagged with consecutive numbers and 3D UTM coordinates (WGS84/ITRF92, grid 14R). Grids on slopes bear imprecisions by vertical projection; we took precautions when measuring inside the grid. The original coordinates were read by three portable GPS devices left outside until they matched, then transported through successive theodolite stations to the datum in the cave, south of X-12 (Fig. 1a, Extended Data Fig. 1d). Each square corner had nails wrapped in yellow tape with coordinates calculated manually, departing from perimetrical values. When gaining depth, the nails were pushed down and verified with the Topcon total station. The *Z* reads for the grid and finds were referred to a datum. Additional datum points were available near the southeastern sector. For finds and depth control, we used a total station, a Sokkia level, levelled strings and measuring tapes. Most items were laser-measured—those moved by the trowel or found by screening were only referred to square or subsquare. All sediment was dry-screened (water screening being impossible) in 3- and 6-mm meshes, under powerful lights. Buckets noted provenience details and the name of the excavator. We used separate bags per material type per subsquare. Few stratum interfaces could be followed along their natural topography (this was nearly impossible in SC-B). Most of the time, we used arbitrary 5- or 10-cm layers, inevitably cross-cutting. Precise measurements allowed us to reconstruct the relative stratigraphic provenience. The strata codes include the excavation number (12), and then consecutive numbers starting with 00 (modern surface). All profiles were inclined, against collapse. We used a stepped approach from both ends, calculating the target depths in relationship to horizontal extension and profile inclination (Fig. 1b, c, Extended Data Figs. 1f–i, 2, Supplementary Information 4). Samples were extracted while digging or later from firm profiles. We used small tools: trowels, spatulas, brushes and so on. Picks and hammers were only allowed for penetrating flowstone. For SC-B, interstrata transitions were largely imperceptible while digging. Therefore, the classification of strata was possible only after macroscopic analysis. However, strata within SC-C were identified and exposed in situ.

Finds recording and management

All finds were recorded at a station installed near the dig. Everything resembling an artefact was collected, avoiding on-the-spot subjectivity. Charcoals for accelerated mass spectrometry (AMS) were immediately given separate codes. Every find bag received a number (1 to 2,168). Each item received inventory numbers. Every find can be identified by the bag number plus inventory number; for example, 206-13456 (bag number-inventory number) (Supplementary Information 1.3). The final processing was done at the University of Zacatecas. If not laser-measured, the finds received 3D UTM coordinates on the basis of provenience and depth, calculated manually, avoiding point overlap. This is why the horizontal distribution of some artefacts has a grid-like artificial look (Extended Data Fig. 3, Supplementary Video 1). Data were plotted with ESRI's ArcMap and ArcScene Geographic Information System (GIS) softwares.

Lithic analysis

The approach was guided by caution to avoid confusion between artefacts and geofacts. Many artefacts could be recognized as such while excavating; others were identified only in the laboratory. Items suggestive of a cultural origin were bagged as lithics. Over 200 kg of lithic material was taken to the laboratory, where 1,930 items were defined as cultural after five rounds of careful study. All pieces discarded as noncultural were kept available for assessment. Lithics were washed by submerging in purified water, without scrubbing, then cleaned with soft brushes and dried indoors. In the analysis, we looked for repeated patterns and shapes, systematic flaking, overlapping scars, prepared platforms and repeated or failed blows, using technological and morphological criteria for the definition of taxa. Inductive references to known Paleoamerican typologies were avoided.

Geology and stratigraphy

Final observations proceeded during a brief visit to Chiquihuite by C.G.O. (November 2017). Field notes of bedrock geology (lithology and structural relationships) inside and outside the cave were compared to the INEGI geological chart G14-10 and publications[36,37]. Examination of profiles involved visual observations of strata and smaller-scale observations of fine- grained units using a hand lens and Dino-Lite digital microscope, allowing better correlations between strata and corrections to previous stratigraphic nomenclatures and interpretations[2,19] (Fig. 1b, Extended Data Fig. 7). Additional studies were completed in Socorro (Supplementary Information 1.1).

Photogrammetry

Creating a 3D model of the excavation X-12 at Chiquihuite Cave presented challenges, including spatial constraints, poor lighting and the scope of the excavation area when contrasted with the necessity of a high-resolution (<0.2-cm) output. These difficulties were compounded by the remote and isolated nature of the field site, which limited lighting options and made modelling in the field unfeasible. A method emphasizing redundancy with limited field equipment is described.

Image data capture was carried out with a Nikon D850 and Nikon AF-S FX 20-mm f/1.8G lens following established methods. Established grids and four prism poles, placed at key points throughout the excavated

area, served as reference scales within the image sets. The location of the excavation presents uneven, undulating, narrow and overhanging surfaces. The recording of these surfaces was made more difficult by poor and contrasting lighting conditions. As the lighting shifts throughout the day, so did corresponding changes in colour temperatures and tonal values. Furthermore, the size of the excavation area enhanced the difficulties in 3D recording, owing to limitations of lumen output from available light sources (strobes and LEDs). Owing to the complexity in both surface topography and limitations in available lighting, two separate sets of stand-alone images were created. The duplication of images offered a contingency for potentially unforeseen lighting limitations and their subsequent effects on 3D geometry and colour values in post-processing. An X-Rite Colour Checker was used for both sets of images, colour corrections were done in post-processing using Adobe Photoshop CC19. The first set of images (set I) consists of 768 images taken at f/11, ISO-200. The camera was placed on a Gitzo carbon-fibre tripod (GK1545T-82TQDUS) to take varying long exposures (ranging from 3″ to 20″) using three battery-operated Ikan Onyx 240 Bi-Colour LED panels set to 4,200 K. The LED panels were hand-held and used to manually light-paint the excavation to the appropriate exposure value. By shooting with a high f-stop and low ISO, the ambient colour values in the cave became negligible owing to underexposure. By using different power outputs on each LED panel, team members assisted in light-painting the entirety of the excavation area. The second set of images (set II) consists of 902 images taken at f/11, 1/125, ISO-200, supplemented with a Nikon SB-900 Speedlight set to TTL metering and −1/3 ev adjustment. The −1/3 ev adjustment reduced the glare and highlights from the varied limestone-based sediments. These images were taken hand-held, which allowed for positions and angles not possible while mounted to a tripod.

For post-processing, raw images were processed in Adobe Photoshop CC19 (version 20.0.2) and exported as JPEGs with sRGB colour profiles at native resolution (8,256 × 5,504). Colour correction was made with X-Rite Colour Checker reference images to establish colour profiles for image sets. The available Adobe Nikon AF-S FX 20-mm f/1.8G correction profile was used to correct vignette and chromatic aberration with distortion correction disabled. Both image sets, totalling 1,670 images, were combined in Agisoft Metashape Pro (version 1.5.1, build 7618) to build model geometry. Images were aligned at high, dense cloud built at medium, and mesh built at high. Texture used only images from set II and output was set to 4,096 resolution at 44 counts. Forty-two reference markers were placed to create 21 scales, cumulatively having a 0.001-m margin of error. The resulting 3D model was exported as a COLLADA file and processed in Blender (v.2.77) to create illustration images (Fig. 1c, Extended Data Fig. 2, Supplementary Information 4).

Petrography

Twelve samples from the 2016–2017 excavations were studied: grey gravels from X-12 (samples M2–M5), light-grey cobble from the slope (M6), slope dark-grey gravel (M7), slope greenish limestone (M8), the dark limestone artefact 1889-12698 (M9), the greenish artefacts 1866-12685, 1899-12709 and 1899-12710 (M10, 11, 12) and the grey artefact 2110-12949 (M13). Later in 2019, three additional samples were obtained from the ceiling of the main entrance (M14), the eastern wall (M15) and the ceiling of the main chamber (M16) (Supplementary Information 1.7). We used a Nikon-Pol200 petrographic microscope (17-megapixel camera). The thin sections went on standard glass slides with EpoThin.

Micromorphology

This was performed on the compacted interface 1210: one sample (M1) extracted by C.G.O from the northwest corner of square I4 (November 2017) by cutting the sediment with trowel and handpick, and wrapping it in adhesive plastic foil on a hard base. Procedures were similar to petrography (Supplementary Information 1.7.1).

Radiocarbon dating

AMS radiocarbon dating of charcoal, bone and sediment was performed at five radiocarbon facilities (Extended Data Table 1): the Oxford Radiocarbon Accelerator Unit (ORAU), Laboratorio de Espectrometría de Masas con Aceleradores (LEMA), Beta Analytic, International Chemical Analysis (ICA) and the PaleoResearch Institute (PRI). The ORAU samples were chemically decontaminated using the acid–base–acid (ABA) protocol for charcoal, ultrafiltration for bone collagen[20] and dated following their protocols[38]. At LEMA, three sediment fractions were obtained when possible: total organic matter, humic acids and a base-insoluble fraction. The former was prepared using acid–alkali–acid treatment[39] and the latter two after different protocols[40]. Bone was prepared according to an approach of collagen extraction[39] based on a modified Longin method[41]. Cleaned samples were converted to graphite in an automated graphitization equipment (AGE 3, Ionplus), and dated following LEMA protocols[42]. Charcoal specks inside sediments were dated as a separate fraction. Processing methods for PRI and Beta Analytic are noted in Supplementary Information 1.8; ICA offers limited protocol information on its website[43]. The calibration of all radiocarbon measurements was done using OxCal 4.3[44] and the IntCal13 calibration curve[45]. The Bayesian age model was created with OxCal 4.3[44], using chronometric data and known stratigraphic information[46] (Fig. 2, Supplementary Information 1.2). 'General' and 'SSimple' outlier models were applied to all remaining chronometric data, and each date was given a 5% prior probability of being an outlier[46]. All dates were rounded to the nearest five years.

OSL dating

Eight samples were initially collected for OSL dating by hammering metal tubes into the face of cleaned sections during archaeological excavations conducted in 2012 and 2016. However, only six samples provided sufficient yields of quartz for optical dating. The samples were processed according to previously described methods[47] and following procedures in use at the luminescence dating laboratory of the Research Laboratory for Archaeology and the History of Art (University of Oxford), further outlined in ref. [48]. These were aimed at isolating sand-sized quartz mineral grains for OSL dating, and independent De estimates were obtained by making standard multi-grain as well as single-grain OSL measurements using luminescence readers manufactured by Risø National Laboratories[49] and Freiberg Instruments[50]. De estimates are based on a conventional single-aliquot regeneration (SAR) measurement protocol[51,52] but to minimize the potential contribution of residual feldspathic components to the quartz signal, each multi-grain OSL measurement was also preceded by an infrared bleach[53,54]. No on-site gamma-ray spectrometry measurements were made and the environmental dose rate was determined from the concentrations of radioisotopes obtained by inductively coupled plasma mass spectrometry using a previously developed dose rate and age calculator[55]. Further details on instrument settings and information pertaining to the OSL measurements and dose-rate calculations of individual samples can be found in Supplementary Information 1.9.

Chemical residues

An exploratory spot test evaluated the potentiality of human-related chemical signatures on the cave floor 1210 (Supplementary Information 1.4). The excavation crew sampled in January 2016, following instructions from the UNAM laboratory. A minimal number of samples achieved satisfactory horizontal coverage in three areas: squares I5 and I6 ($n = 15$), G2 and H2 (16), and J3 and K3 (12). We installed metric grids with measuring tapes, marking sampling spots with paper tags, 50 cm apart. Sediment samples were extracted with clean metal spoons and placed in polyethylene bags. All samples were tested for phosphates, carbonates, protein, fatty acids and carbohydrates residues following UNAM procedures[56]. Semiquantitative results were plotted

on distribution maps where colour saturation indicates higher values of each indicator. The X-ray fluorescence equipment had a 75-W tungsten X-ray tube, Si-PIN Amptek detector and Spellman high voltage source. All measurements met the same conditions—35 kV, 0.11 mA and 420 s)—to directly compare the spectra. Counts were measured for each chemical element using Pymca software and transformed into an arbitrary 1-to-5 range to configure maps.

Pollen and phytoliths

Nine 1-kg sediment samples were extracted during the excavation (January 2017) for testing the palaeoenvironmental potential of the site. As we were unable to use columns, the samples were obtained horizontally while digging, from across the eastern half of square M3 and western N3, keeping a column-like vertical relationship between them (Supplementary Information 1.6). Each sample corresponded to a 10-cm layer, inevitably cross-cutting strata. Each one provided three different subsamples for phytolith analysis and two independent pollen assessments. At the São Paulo laboratory, phytoliths were extracted from 100 ml of sediment following the wet oxidation method[57]. The sediment was sieved into silt and sand fractions, the residue was mounted in Permount mounting medium, and phytoliths counted under 400× (silt) and 200× (sand). A phytolith count of 200 was sought in each sample and graphs were made using C2 software. Grass short-cell phytoliths were identified according to published Poaceae reference collections[58–60]. For pollen, samples were sieved for gravel removal (>250 µm) and 5 cm^3 of sediment was processed for pollen grains[61]. A final sieving stage (5 µm) was added to remove clay, using two *Lycopodium* sp. tablets per sample. Samples were counted under 100× using immersion oil and 150+ palynomorphs counted. For both studies, photographs were taken with Zen software. Percentage and concentration values were calculated and plotted using TILIA (TILIAGRAPH). Pollen identification was made with in-house reference collections and through comparison with South American and Mexican publications[31,62–66] (Supplementary Information 1.6). At Mexico City, the ENAH laboratory used chlorhydric acid to dissolve carbonates and sodium hexametaphosphate to disaggregate particles such as silt and clay from the sand. *Lycopodium* pills were added, and then acetolysis took place. Flotation was made with CsCl (density: 1.9) and samples were counted and photographed, both at 100×. Graphs were made with C2 version 1.7.7.

Environmental DNA

We collected bulk sediment samples from 15 stratigraphic locations in which some layers were assumed to be exposed to human activity before becoming buried (Extended Data Figs. 2a, b, Supplementary Information 1.10, 2–4). The samples were transferred to clean either sterile 50-ml spin tubes or 0.5-l plastic containers using sterile disposable scalpels or cleaned metal spoons, while wearing a face mask, full-body suit and nitrile gloves. Samples were sent to Copenhagen and stored at −20 °C until further subsampling and extraction. Subsamples (approximately 5 g) were collected from each of the sampled layers in laboratories exclusively dedicated to ancient DNA, at the Globe Institute (University of Copenhagen), removing gravel and stones. Subsamples from three layers of the first extraction batch were then subjected in parallel to two different lysis buffers; to the first was added 5 ml of 1M Tris-HCl and 230µg proteinase-K based buffer ('Sergey Bulat buffer')[30], and to the second was added 5 ml sodium phosphate buffer with 500 µl MT buffers both from the FastDNA spin kit for soil from MPBio together with 230 µg proteinase K ('Extraction buffer test' in Supplementary Information 1.10.3). All samples were vigorously shaken to lyse and release DNA from tissue and minerals, using a FastPrep at 4.5 ms in 40 s and thereafter incubated gently rotating overnight at 37 °C. All samples were then spun at 4,000*g* in 15 min and the supernatant was transferred to a new sterile 15-ml spin filters.Ten millilitres UltraPure phenol:chloroform:isoamyl alcohol (25:24:1) were added to the supernatant to denature and separate proteins and phenols, and incubated at room temperature for 10 min while gently rotating. All samples were then spun down at 4,000*g* for 5 min and the supernatant transferred to 10-kDa Amicon Ultra-15 filters. The samples were then spun at 4,000*g* to a 200-µl volume and washed twice with 1.0 ml Qiagen EB buffer and spun to a 200-µl volume. The final retentate were then transferred to a sterile low-bind Eppendorf tube and stored at −20 °C until it was converted to a multiplexed dual-indexed Illumina library using standard protocol[67]. The libraries were then sequenced on Illumina HiSeq 2500, 4000, or the NocaSeq 6000 platform using 80-basepair single-read or 100-basepair paired-end for the NovaSeq, respectively. We generated a total of 3,736,476,081 raw reads after demultiplexing and adaptor removal. All single-end reads and collapsed reads from the NoveSeq were parsed through the pipeline 'Holi' for quality control[30], removal of low-complexity reads, duplicates and reads below 30 bp in size (Supplementary Information 1.10). This resulted in a total of 1,500,645,904 reads being parsed for alignment against the full NCBI nt (release 228) as well as the complete non-redundant RefSeq database (downloaded November 2018), and eventually parsed through ngsLCA, a naive least common ancestor algorithm that parses only reads with 100% similarity to the reference for taxonomic assignment. This resulted in between 6,784 and 869,776 unique taxonomic identification distributed on each layer and 59,912 taxonomic identifications for all the controls. All taxa found in the controls with two or more reads were subtracted from the complete dataset. The taxonomic unit with >1 read and were parsed to R and plotted in ordination space using packages ggplot2 and gplot. The dataset was divided into the kingdoms Amniota and Viridiplantae with the lowest taxonomic nodes at genus level applying a cut-off threshold for each taxonomic unit of 1% within each kingdom. All plant and animal genera found were screened for DNA damage using the reference genome from the most abundant species found by Holi for each genus[68]. We next parsed only reads uniquely classified within each genus and kept only taxa with DNA damage >0.10 C-T frequencies at the 3′ end (metadata file). The distribution of read lengths, the edit distance reference genome and the 3′ DNA damage were plotted in R (Supplementary Information 2, 3). The final genus lists were then plotted using R packages, rioja, ggplot2 and gplot, combined and layout finalized in Illustrator (Extended Data Fig. 4, Supplementary Information 1.10). Further determination of the presence of ancient human DNA was carried out by mapping sequencing reads of each sample against two different reference indices: the human reference genome (build GRCh38Decoy); and all mitochondrial genomes from RefSeq (release 92). Reads were mapped using bowtie2 (version 2.3.2) in end-to-end mode, using the 'very-sensitive' preset and allowing for an additional mismatch for seed alignment (command line parameters -D 20 -R 3 -N 1 -L 20 -i S,1,0.50 --end-to-end). Final-analysis BAM files were obtained by applying mapping quality (MQ) filter MQ ≥ 25 following duplicate removal (Supplementary Information 1.10).

Reporting summary

Further information on research design is available in the Nature Research Reporting Summary linked to this paper.

Data availability

The data that support the findings of this study are available in the Article and its Supplementary Information. Raw data and sequence alignments are available from the European Nucleotide Archive under accession number PRJEB37914. The exact coordinates of Chiquihuite Cave are available from C.F.A. on reasonable request. C.F.A. can also be contacted at cip_ardelean@hotmail.com.

Code availability

Code for R and OxCal is noted within the Supplementary Information. Code for environmental DNA data analysis can be found at https://github.com/miwipe/ngsLCA.

36. Sedlock, R. L., Ortega-Gutiérrez, F. & Speed, R. C. *Tectonostratigraphic Terranes and Tectonic Evolution of Mexico (GSA Special Papers Volume 278)* (Geological Society of America, 1993).
37. Padilla y Sánchez, R. J. *Geological Map of the Curvature of Monterrey, Mexico* (GSA, 2006).
38. Ramsey, C. B., Higham, T. & Leach, P. Towards high-precision AMS: progress and limitations. *Radiocarbon* **46**, 17–24 (2004).
39. Hajdas, I. Radiocarbon dating and its applications in Quaternary studies. *E&G Quat. Sci.J.* **57**, 2–24 (2008).
40. Abbott, M. B. & Stafford, T. W. Radiocarbon geochemistry of modern and ancient Arctic lake systems, Baffin Island, Canada. *Quat. Res*. **45**, 300–311 (1996).
41. Longin, R. New method of collagen extraction for radiocarbon dating. *Nature* **230**, 241–242 (1971).
42. Solís, C. et al. A new AMS facility in Mexico. *Nucl. Instrum. Methods Phys. Res. B* **331**, 233–237 (2014).
43. International Chemical Analysis. *International Chemical Analysis*. https://www.radiocdating.com/ (accessed 18 July 2018) (2017).
44. Bronk Ramsey, C. Bayesian analysis of radiocarbon dates. *Radiocarbon* **51**, 337–360 (2009).
45. Reimer, P. J. et al. IntCal13 and Marine13 radiocarbon age calibration curves 0–50,000 years cal BP. *Radiocarbon* **55**, 1869–1887 (2013).
46. Bronk Ramsey, C. Dealing with outliers and offsets in radiocarbon dating. *Radiocarbon* **51**, 1023–1045 (2009).
47. Aitken, M. J. *Introduction to Optical Dating: The Dating of Quaternary Sediments by the Use of Photon-stimulated Luminescence* (Clarendon, 1998).
48. Mirazón Lahr, M. et al. Inter-group violence among early Holocene hunter-gatherers of West Turkana, Kenya. *Nature* **529**, 394–398 (2016).
49. Bøtter-Jensen, L., Bulur, E., Duller, G. A. T. & Murray, A. S. Advances in luminescence instrument systems. *Radiat. Meas*. **32**, 523–528 (2000).
50. Richter, D., Richter, A. & Dornich, K. Lexsyg smart—a luminescence detection system for dosimetry, material research and dating application. *Geochronometria* **42**, 202–209 (2015).
51. Murray, A. S. & Wintle, A. G. Luminescence dating of quartz using an improved single-aliquot regenerative-dose protocol. *Radiat. Meas*. **32**, 57–73 (2000).
52. Wintle, A. G. & Murray, A. S. A review of quartz optically stimulated luminescence characteristics and their relevance in single-aliquot regeneration dating protocols. *Radiat. Meas*. **41**, 369–391 (2006).
53. Banerjee, D., Murray, A. S., Bøtter-Jensen, L. & Lang, A. Equivalent dose estimation using a single aliquot of polymineral fine grains. *Radiat. Meas*. **33**, 73–94 (2001).
54. Wallinga, J., Murray, A. S. & Bøtter-Jensen, L. Measurement of the dose in quartz in the presence of feldspar contamination. *Radiat. Prot. Dosimetry* **101**, 367–370 (2002).
55. Durcan, J. A., King, G. E. & Duller, G. A. T. DRAC: dose rate and age calculator for trapped charge dating. *Quat. Geochronol*. **28**, 54–61 (2015).
56. Barba, L. Chemical residues in lime-plastered archaeological floors. *Geoarchaeology* **22**, 439–452 (2007).
57. Piperno, D. R. *Phytoliths: A Comprehensive Guide for Archaeologists and Paleoecologists* (Rowman Altamira, 2006).
58. Piperno, D. R. & Pearsall, D. M. *The Silica Bodies of Tropical American Grasses: Morphology, Taxonomy, and Implications for Grass Systematics and Fossil Phytolith Identification* (Smithsonian Institution, 1998).
59. Gallego, L. & Distel, R. A. Phytolith assemblages in grasses native to central Argentina. *Ann. Bot*. **94**, 865–874 (2004).
60. Fredlund, G. G. & Tieszen, L. T. Modern phytolith assemblages from the North American Great Plains. *J. Biogeogr*. **21**, 321–335 (1994).
61. Colinvaux, P., De Olieira, P. E. & Moreno Patino, J. E. *Amazon Pollen Manual and Atlas* (Harwood Academic, 1999).
62. Roubik, D. W. & Moreno Patiño, J. E. *Pollen and Spores of Barro Colorado Island* (Missouri Botanical Garden, 1991).
63. Markgraf, V. & d'Antoni, H. L. *Pollen Flora of Argentina* (Univ. Arizona Press, 1978).
64. Johnston, I. M. Plants of Coahuila, eastern Chihuahua, and adjoining Zacatecas and Durango, *V. J. Arnold Arbor*. **25**, 133–182 (1944).
65. González-Tagle, M. A., Schwendenmann, L., Pérez, J. J. & Schulz, R. Forest structure and woody plant species composition along a fire chronosequence in mixed pine–oak forest in the Sierra Madre Oriental, Northeast Mexico. *For. Ecol. Manage*. **256**, 161–167 (2008).
66. Ludlow Wiechers, B., Almeida Leñero, L. & Sugiura, Y. Palinomorfos del Holoceno en la cuenca alta del Río Lerma, Estado de México, México. *Bol. Sociedad Botánica de México* **72**, 59–105 (2003).
67. Meyer, M. & Kircher, M. Illumina sequencing library preparation for highly multiplexed target capture and sequencing. *Cold Spring Harb. Protoc*. **2010**, db.prot5448 (2010).
68. Jónsson, H., Ginolhac, A., Schubert, M., Johnson, P. L. F. & Orlando, L. mapDamage2.0: fast approximate Bayesian estimates of ancient DNA damage parameters. *Bioinformatics* **29**, 1682–1684 (2013).

Acknowledgements The field explorations and part of the laboratory studies were made possible by the special sponsorship from the Government of the State of Zacatecas, through the Consejo Zacatecano de Ciencia, Tecnología e Innovación (COZCyT); we thank its consecutive directors, G. A. Mercado-Sánchez and A. Enciso-Muñoz, and the Governor of Zacatecas, A. Tello-Cristerna. Seed money for cave exploration came from the Center for American Paleolithic Research (CAPR); we thank S. Holen, K. Holen and the members of the board. Fieldwork, laboratory analyses and publication expenses were partially covered by CONACYT grant CB-2016-286130. The Concepción del Oro municipality, and A. Maldonado-Falcón, offered administrative and occasional financial assistance. Radiocarbon work at Oxford was supported by the NERC Radiocarbon Facility (NRCF), Merton College, Santander and the Clarendon Fund. We thank all colleagues at the ORAU. D. Peat contributed greatly to laboratory preparation of OSL samples. A. Ocaña and I. Alarcón participated in the identification of animal bones. The environmental DNA work was supported by the Lundbeck Foundation, the Novo Nordic Foundation, the Wellcome Trust Foundation, the Carlsberg Foundation and the Danish National Research Foundation. We thank INAH's Archaeology Council for authorization and legal permits; the inhabitants of Guadalupe Garzarón for accepting this project in their territory and participating in the caravans; and J. Martínez-Ledezma for his constant support as an on-site administrator and liaison with the community.

Author contributions C.F.A. designed the project, directed excavations, analysed lithics, photographed artefacts and put together the research team. L.B.-V. and T.H. performed sampling, AMS radiocarbon dating and Bayesian modelling analysis. C.S.-R. and M.R.-C. performed AMS radiocarbon dating. M.W.P., M.S. and E.W. designed and conducted the DNA and bioinformatic analyses. J.-L.S. undertook the OSL dating. C.G.O. performed geological studies. J.I.M.-Q. participated in the discovery of the site, mapping, artefact plotting and GIS analyses. J.A.-C. conducted the zooarchaeological analysis. L.B.-P. and A.O.-B. conducted chemical residues analysis. J.B.-V. performed X-ray fluorescence. Y.Z.E.O.-D. and I.I.R.-C. conducted thin-section petrography and micromorphology analyses. J.G.W. performed the phytolith analysis. V.B.d.M., P.E.D.O. and I.R.-G. studied pollen samples. Z.N.-G. performed flotation and malacology analyses. D.A.G. performed photogrammetry. Z.N.-G., J.J.D.L.R.-D., V.H.-A., M.B.M.-F., L.M.M.-R., and A.L.-J. excavated. C.F.A., L.B.-V., M.W.P., J.I.M.-Q., J.J.D.L.R.-D. and D.A.G. created figures. C.F.A. wrote the paper with co-authors contributing to the draft.

Competing interests The authors declare no competing interests.

Additional information

Supplementary information is available for this paper at https://doi.org/10.1038/s41586-020-2509-0.

Correspondence and requests for materials should be addressed to C.F.A. or E.W.

Peer review information *Nature* thanks Deborah M. Pearsall, Fiona Petchey and the other, anonymous, reviewer(s) for their contribution to the peer review of this work.

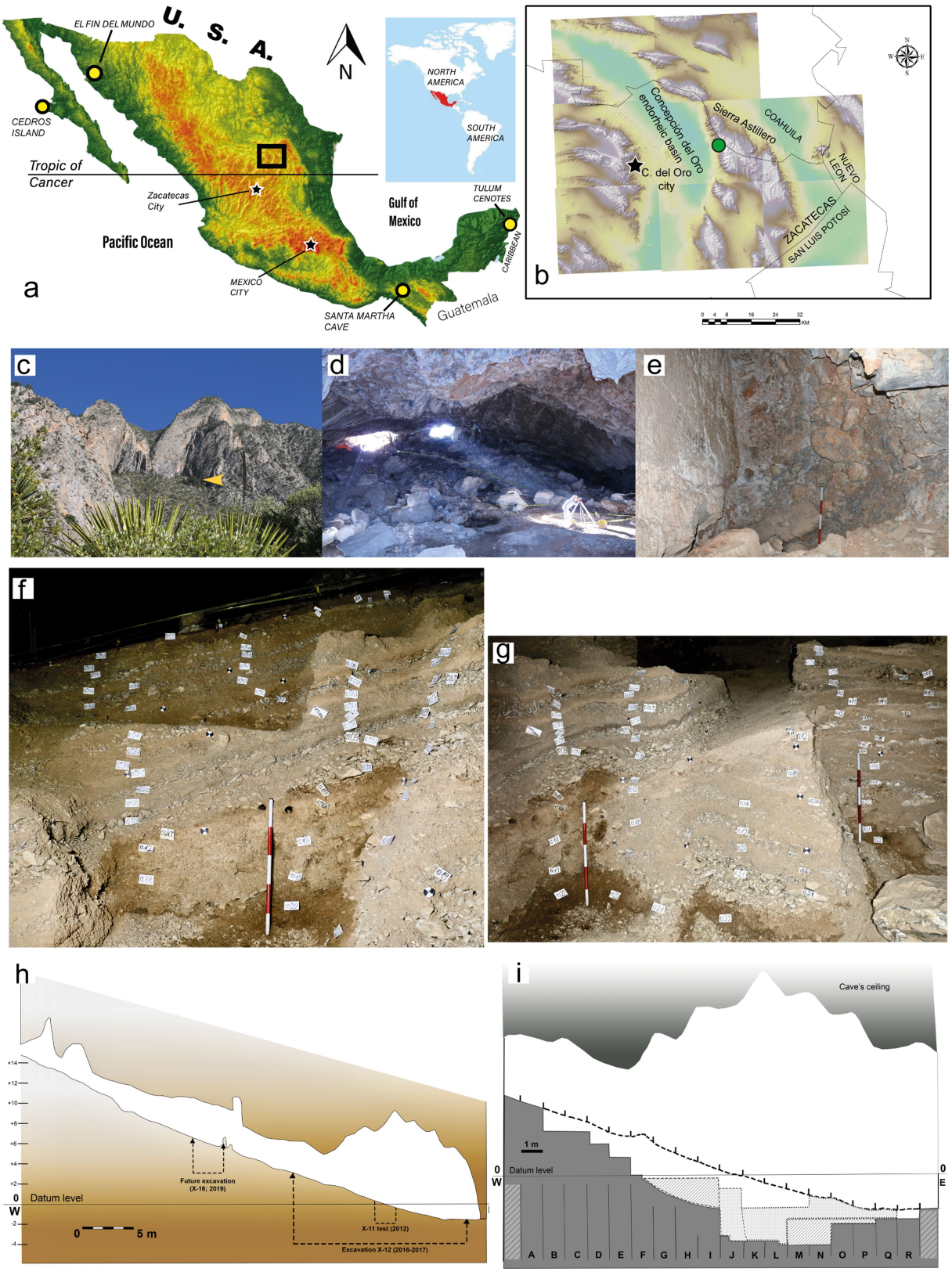

Extended Data Fig. 1 | See next page for caption.

Extended Data Fig. 1 | Additional information on the site and excavation. **a**, Digital elevation model (DEM) map of Mexico with the study area (rectangle) in relationship to relevant modern and prehistoric localities. **b**, The study region (Concepción del Oro endorheic basin), with Chiquihuite Cave (green dot) on the Astillero Mountains. DEM mosaic generated from ortophotographs and elevation data from National Institute of Statistics and Geography (INEGI) of Mexico. **c**, Chiquihuite Peak, seen from the south; the arrow indicates the entrance of the cave. **d**, The main chamber, looking west towards the double-eyed entrance. **e**, Contact between the limestone lintel of the ancient entrance (25 m west of X-12), and the debris that sealed it, probably at the end of the Pleistocene epoch. **f**, The south profile of the central–eastern squares, as in Fig. 1b. **g**, Western profiles of the central sector, showing the exposed interface 1210 tilted in the centre of the photograph. **h**, East–west cross-section of the northern sector of the main chamber of the cave, along the southern profile of the dig. **i**, X-12 cross-section, showing the inclination of the cave floor and the stepped approach. The DEMs in **a**, **b** were created with ArcMap/ArcScene (by ESRI) using open-access topographical data provided by INEGI.

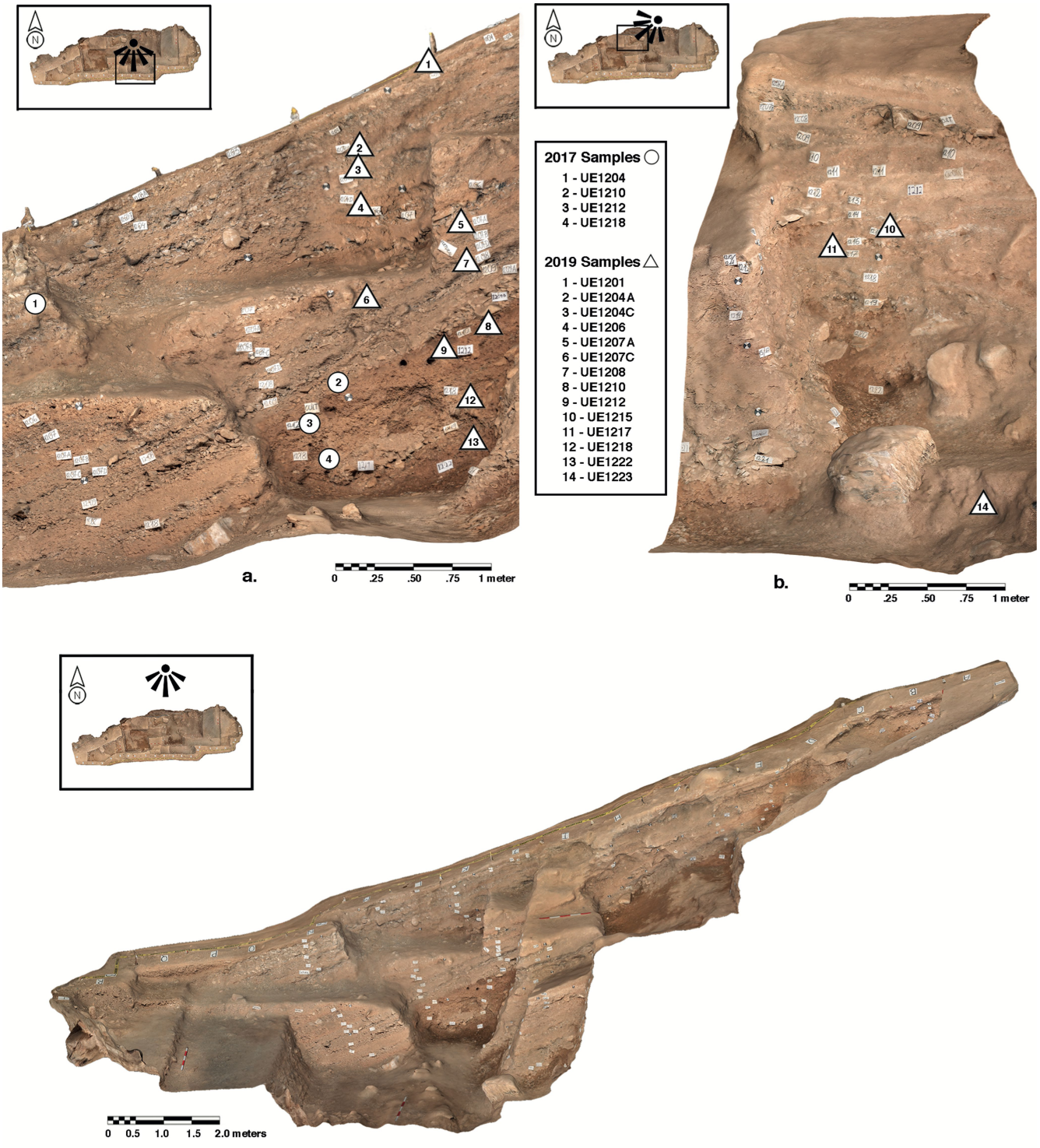

Extended Data Fig. 2 | Three-dimensional photogrammetric model of excavation X-12 and the location of samples extracted and analysed for ancient environmental DNA. a, North-facing profile. **b**, East-facing profile. Triangles indicate the respective locations of environmental DNA samples extracted in 2019, corresponding to different stratigraphic units ('UE', as shown in the key). The circled samples are the initial ones, from the 2016–2017 excavation. **c**, Complete 3D photogrammetric view of the excavation towards the southern profile. The reddish-brown layers visible along the entire southern profile represent the stratigraphic component C (SC-C), starting downwards with stratum 1212, the terminal LGM chronostratigraphic marker that defines the separation between SC-B and SC-C (Fig. 1b, Extended Data Fig. 7).

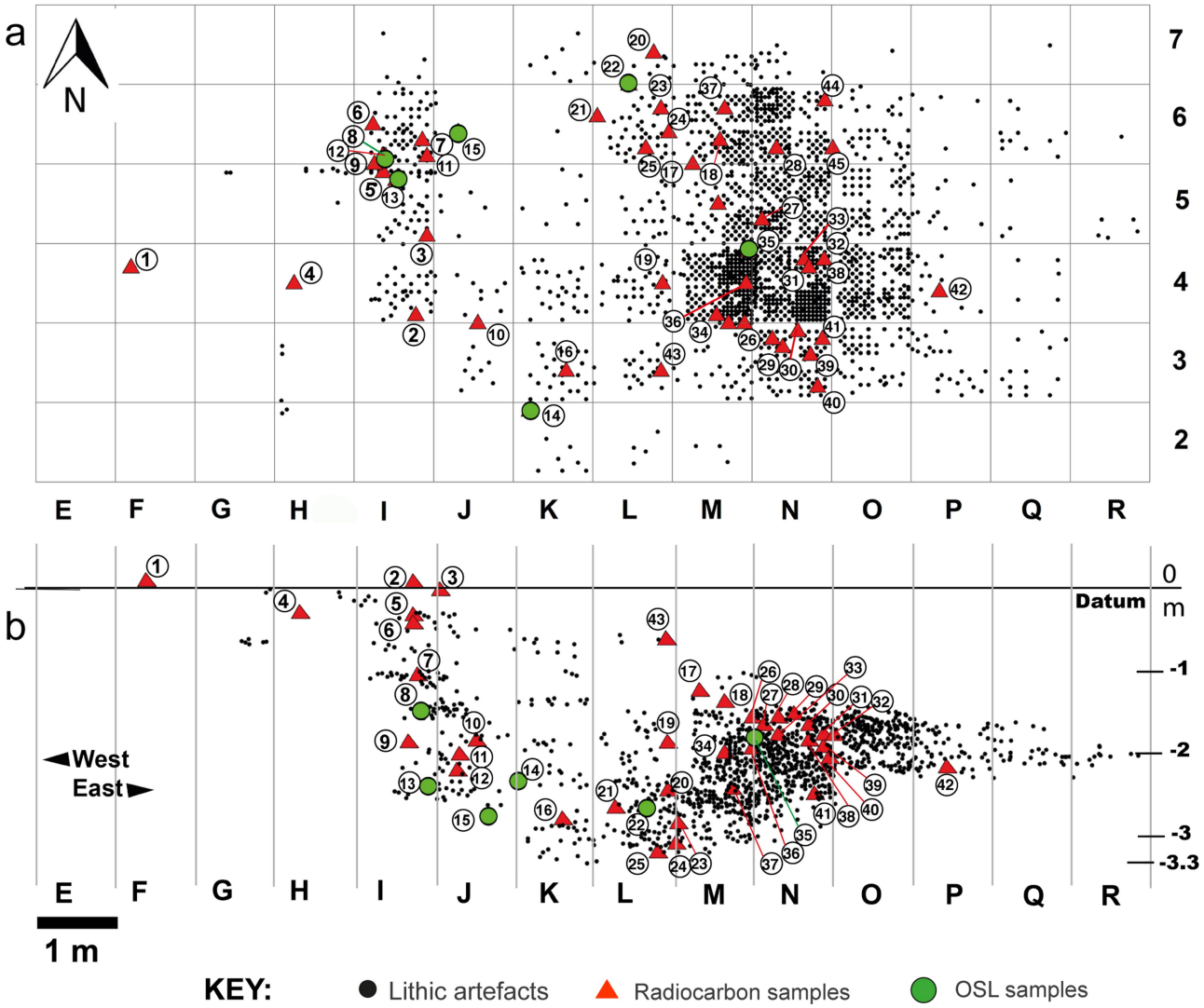

Extended Data Fig. 3 | Finds plotted onto the excavation grid. a, Horizontal (*x* and *y* axes) spatial distribution of lithic artefacts, radiocarbon and OSL samples on the excavation grid. **b**, Side view (from the south) of the vertical distribution (*x* and *z* axes) of finds and samples. Illustrated dating samples: (1) LEMA-635.1.1 and LEMA-635.1.2; (2) OxA-36608 and LEMA-978.1.1; (3) OxA-36610; (4) LEMA-574.1.1; (5) LEMA-640.1.1; (6) OxA-36496; (7) OxA-36613; (8) X-7227; (9) OxA-36614; (10) LEMA-636.1.1 and LEMA-636.1.2; (11) LEMA-576.1.1; (12) LEMA-577.1.1; (13) X-7228; (14) X-7231 and X-7232; (15) X-7229; (16) OxA-36530; (17) OxA-36633; (18) OxA-36609; (19) OxA-36612; (20) OxA-36360; (21) BETA-345055; (22) X-4135; (23) OxA-34965; (24) ICA-16OS/0510; (25) PRI-5414; (26) OxA-36616; (27) OxA-36620; (28) OxA-36618; (29) OxA-36615; (30) OxA-36617; (31) OxA-36621; (32) OxA-36619; (33) OxA-36753; (34) OxA-36611; (35) X-7233; (36) LEMA-573.1.1; (37) OxA-36359; (38) LEMA-892.1.2; (39) OxA-36622; (40) OxA-36623; (41) OxA-36634; (42) LEMA-893.1.1; (43) LEMA-977.1.1; (44) OxA-36624; and (45) OxA-36625.

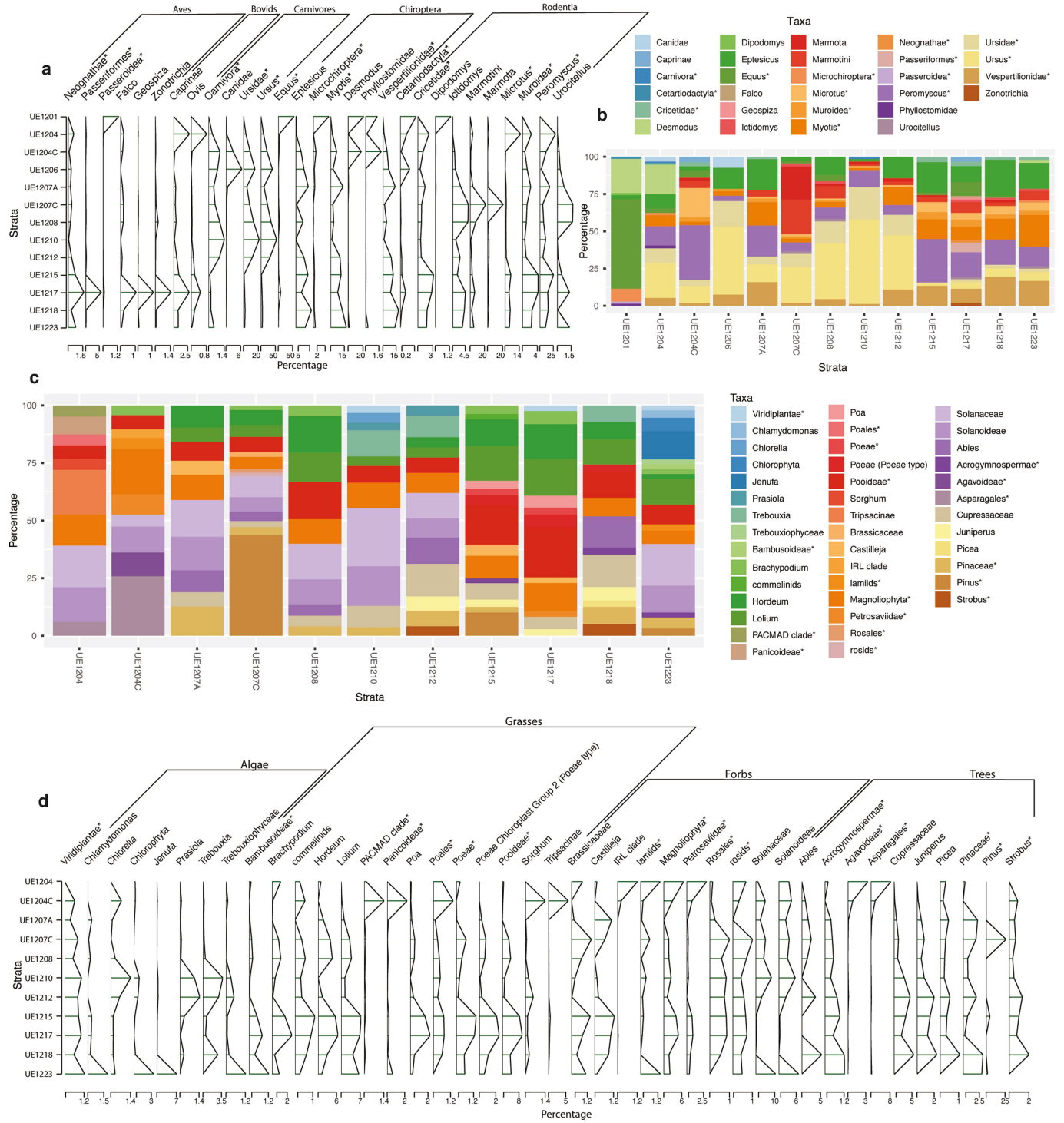

Extended Data Fig. 4 | Taxonomic profiles of animals (Amniota) and plants (Viridiplantae) identified by ancient environmental DNA. a, **b**, Animals presented as the proportion of reads found of each taxa and plotted as a bar plot (**b**) and stratigraphic plot (**a**). **c**, **d**, All plants are presented as the proportion of reads found of each taxa and plotted as a bar plot (**c**) and stratigraphic plot (**d**). *Taxa also found by pollen, phytoliths or faunal remains.

Extended Data Fig. 5 | Additional Chiquihuite lithic artefacts. a–**c**, Cores. **d**, **e**, Bifacial preforms on ovoid nodules. **f**–**n**, Flakes. **o**–**t**, Blades. **u**–**x**, Microliths. **y**, **w**, Burins. **z**, **a′**, Scrapers. **b′**–**l′**, Points and point-like shapes. **m′**–**p′**, Geometric items made by fracturing calcite laminae. Artefacts **i**, **n**, **o**, **b′**, **c′**, **f′**, and **k′** are from SC-C; all others are from SC-B. Scale bars, 1 cm.

Extended Data Fig. 6 | Additional examples of lithics. a, Core. **b**, Flake with isolated platform. **c**, Flake with lipped platform. **d**–**i**, Blades and microlith blade segments. **j**, Circular scraper on trimmed flake. **k**, Possible preform. **l**, Point on plaquette. **m**, Bifacial point preform. **n**, **o**, **s**–**a′**, **d′**–**g′**, Transversal points (obtained by slightly modifying transversal flake blanks). **p**–**r**, **b′**, **c′**, Other points. **h′**, A geometric, point-like shape on calcite sheet. Most artefacts were discovered in SC-B. Specimens **x**–**z**, **b′**, **g′**, **h′** are from SC-C. Scale bars, 1 cm.

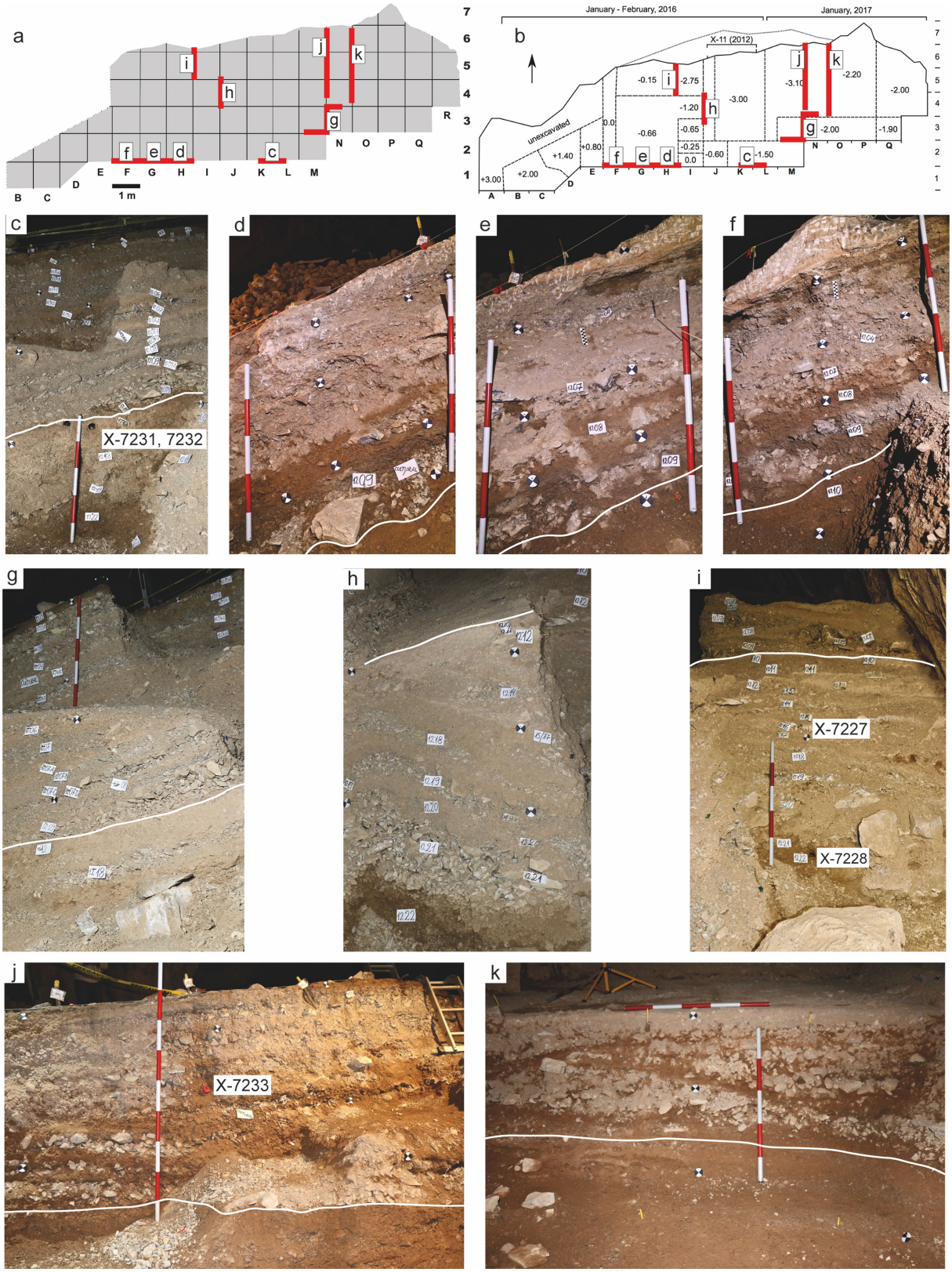

Extended Data Fig. 7 | Stratigraphic correlations across different profiles in X-12. a, **b**, Excavation grid diagram (**a**) and maximum-depth diagram (**b**) showing the position of the profiles depicted below. For correlation reasons, all profiles show the upper contact of stratum 1210 with 1212 marked with a white contour. The position of OSL samples is indicated (labels beginning with X-). **c**, South profile, squares K2, K3, L2 and L3. **d**, South profile, square H2. **e**, South profile, square G2. **f**, South profile, square F2. **g**, South profile, squares M3, M4, N3 and N4. **h**, West profile, square J4. **i**, West profile, squares I5 and I6. **j**, Eastern profile, squares M4, M5 and M6 (profile removed during the 2016–2017 winter excavations). **k**, Eastern profile, squares N4, N5 and N6 (new eastern profile after the excavation of the one shown in **j**).

Extended Data Table 1 | Chronometric data ordered by strata and depth

Strat. comp.	Stratum	Depth (m) from datum	Square	Sample (field number)	Laboratory code	Dating method	Material	Taxon	% Collagen yield	C:N	%C	$\delta^{13}C$‰	$\delta^{15}N$‰	Date (^{14}C years BP)	cal BP (95.4% confidence level) or OSL age
A	1201	-0.57	L3	#1-8830	LEMA-977.1.1	^{14}C-AMS	Bone	faunal	4.3	2.9	42.6	-15	-	237±35	430-0
B	1204 upper interface	-0.89	M3	1-B	LEMA-978.1.1	^{14}C-AMS	Charcoal	-	-	-	44.6	-23	-	10,513±50	12,650-12,185
B	1204 upper interface	0.07	I4	1	OxA-36608	^{14}C-AMS	Charcoal	-	-	-	58	-21.6	-	12,060±50	14,065-13,760
B	1204	-0.35	I5/I6	i5/6-#255	LEMA-640.1.1	^{14}C-AMS	Bone	faunal	1.4	1	17.7	-29	-	11,403±60	13,385-13,105
B	1204 ABC	-1.82	N4-NE	85	LEMA-892.1.2	^{14}C-AMS	Charcoal	-	-	-	60.5	-20	-	11,770±35	13,725-13,475
B	1204	-1.65	N6-SW	76	OxA-36618	^{14}C-AMS	Charcoal	*Pseudotsuga*	-	-	61.1	-25.1	-	11,855±50	13,770-13,560
B	1204	-1.74	N4-NE	82	OxA-36621	^{14}C-AMS	Charcoal	*Pinus*	-	-	61.3	-23.7	-	11,890±45	13,790-13,565
B	1204	-0.01	I5-SW	16	OxA-36610	^{14}C-AMS	Charcoal	-	-	-	63.2	-23.7	-	11,895±50	13,815-13,555
B	1204	-2.09	P4-SW	93	LEMA-893.1.1	^{14}C-AMS	Charcoal	-	-	-	70.7	-24	-	11,897±35	13,785-13,575
B	1204 D	-1.96	N6-NE	88	OxA-36624	^{14}C-AMS	Charcoal	-	-	-	61.9	-24.8	-	11,900±50	13,835-13,555
B	1204	-1.65	N3-NE	73	OxA-36753	^{14}C-AMS	Charcoal	*Cupressaceae*	-	-	53.3	-22.3	-	11,975±70	14,035-13,600
B	1204 D	-0.44	I6	#246-9477	OxA-36496	^{14}C-AMS	Bone (Extnd. Fig. 5f)	faunal	1.5	3.2	43.1	-20.9	8.5	12,005±55	14,030-13,735
B	1204/ 1204 ABC	-1.68	N3-NE	77	OxA-36619	^{14}C-AMS	Charcoal	*Pseudotsuga*	-	-	61.7	-23.5	-	12,040±50	14,045-13,755
B	1204	-1.47	N4-SW	70	OxA-36616	^{14}C-AMS	Charcoal	*cf. Abies*	-	-	62.6	-23.9	-	12,050±50	14,055-13,760
B	1204	-1.41	N3-NW	69	OxA-36615	^{14}C-AMS	Charcoal	*Pinus*	-	-	62.7	-23.9	-	12,095±50	14,105-13,775
B	1204	-1.55	N3-NE	71	OxA-36617	^{14}C-AMS	Charcoal	*Cupressaceae*	-	-	56.2	-23.5	-	12,120±50	14,105-13,775
B	1204 ABC	-1.45	M6	6	OxA-36609	^{14}C-AMS	Charcoal	*Pinus*	-	-	65.2	-24.1	-	12,120±50	14,140-13,795
B	1204	-1.7	N5-SW	81	OxA-36620	^{14}C-AMS	Charcoal	*Abies*	-	-	62.8	-24.3	-	12,140±50	14,165-13,820
B	1204	-1.75	N3-NE	83	OxA-36622	^{14}C-AMS	Charcoal	*Pseudotsuga*	-	-	59.8	-22.3	-	12,155±50	14,185-13,835
B	1204 D	-1.95	N6-SE	89	OxA-36625	^{14}C-AMS	Charcoal	*Pinaceae*	-	-	64	-24.9	-	12,170±50	14,205-13,855
B	1204	-1.3	M6-SW	5	OxA-36633	^{14}C-AMS	Chacoal	-	-	-	61.8	-21.8	-	12,235±75	14,570-13,855
B	1204 lower	-1.8	M4-N / N4-N	OSL 5	Oxford X-7233	OSL	Sediment	-	-	-	-	-	-	10,960±1,610	N/A
B	1206	-1.85	N3-SE	86	OxA-36623	^{14}C-AMS	Charcoal	*Pseudotsuga*	-	-	60.4	-25.1	-	13,010±55	15,790-15,315
B	1207	-2.05	M5-C	26	Beta-436710	^{14}C-AMS	Charcoal	-	-	-	*	-22.7	-	12,880±50	15,605-15,180
B	1207	-1.8	L4-E	23	OxA-36612	^{14}C-AMS	Charcoal	-	-	-	61.5	-25.1	-	12,885±50	15,615-15,185
B	1207	-1.9	M4-E	20	LEMA-573.1.1	^{14}C-AMS	Charcoal	-	-	-	51.8	-29	-	12,916±58	15-680-15-215
B	1207	-2.45	N3-NE	100	OxA-36634	^{14}C-AMS	Charcoal	*Pinus*	-	-	63.3	-22.3	-	12,990±55	15,760-15,300
B	1207	-0.28	H4-NW	25	LEMA-574.1.1	^{14}C-AMS	Charcoal	-	-	-	61.2	-29	-	13,092±63	15,955-15,400
B	1209	-1.9	M4-S	22	OxA-36611	^{14}C-AMS	Charcoal	-	-	-	62.6	-23.9	-	13,050±55	15,850-15,360
B	1209 supra 1210	0.1	F4-NW	15	LEMA-635.1.1	^{14}C-AMS	Charcoal	-	-	-	61.5	-19	-	13,054±60	15,875-15,345
B	1209	-2.65	M6-NE	#2012-15345	OxA-36359	^{14}C-AMS	Bone	faunal	6.6	3.2	41.7	-12.1	7.9	13,525±35	16,500-16,125
B	1209 supra 1210	0.1	F4-NW	15 replica	LEMA-635.1.2	^{14}C-AMS	Charcoal	-	-	-	58	-21	-	13,142±60	16,030-15,545
B	1209 supra 1210	-1.1	I6-SE	30	OxA-36613	^{14}C-AMS	Charcoal	-	-	-	58.5	-24	-	13,630±55	16,670-16,210
B/C transit	interface 1210	variable, following stratum	G4 / H4	29A	Beta-436709	^{14}C-AMS	Sediment	-	-	-	*	-20.2	-	13,010±50	15,780-15320
B/C transit	interface 1210	-1.77	J4-S/SW	37	LEMA-636.1.1	^{14}C-AMS	Charcoal	-	-	-	60	-18	-	13,569±60	16,600-16,140
B/C transit	interface 1210	-1.77	J4-S/SW	37 rep	LEMA-636.1.2	^{14}C-AMS	Charcoal	-	-	-	61.7	-24	-	13,788±90	16,995-16,930
B/C transit	interface 1210	variable, following stratum	G4 / H4	29B	LEMA-575.1.2	^{14}C-AMS	Sediment	-	-	-	4.8	-24	-	14,107±64	17,430-16,925
B/C transit	interface 1210	variable, following stratum	G4 / H4	29B rep	LEMA-575.1.3	^{14}C-AMS	Charcoal	-	-	-	4	-23	-	14,778±77	18,215-17,750
B/C transit	1210	-2.08	K3 south profile	OSL 4A	Oxford X-7231	OSL	Sediment	-	-	-	-	-	-	15,560±1,740	N/A
B/C transit	1212	-2.1	K3 south profile	OSL 4B	Oxford X-7232	OSL	Sediment	-	-	-	-	-	-	13,870±2,250	N/A
C	1217	-1.55	I6-W	OSL 1A	Oxford X-7227	OSL	Sediment	-	-	-	-	-	-	11,620±2,000	N/A
C	1218-1219	-2	I6-SW	39	OxA-36614	^{14}C-AMS	Charcoal	*Pseudotsuga*	-	-	59.2	-24.1	-	20,860±100	25,525-24,795
C	1218-1219	-2.75	L7-SE	#2061-15346	OxA-36360	^{14}C-AMS	Bone (Extnd. Fig. 5a)	faunal (*Gymnogyps* sp.?)	5	3.2	44	-13.6	14.2	21,140±130	25,770-25,180
C	1219	-3.07	L6	L6-#569	OxA-34965	^{14}C-AMS	Bone	faunal	7.6	3.2	41.1	-19.4	5.5	21,990±170	26,635-25,880
C	1219	-2.6	K3-C	#520-9976	OxA-36530	^{14}C-AMS	Bone (Extnd. Fig. 5d)	faunal	5.3	3.3	44.3	-14.8	8.9	22,170±140	26,840-26,030
C	1220	-2.16	I6-SE	49	LEMA-576.1.1	^{14}C-AMS	Charcoal	-	-	-	55.3	-26	-	20,896±80	25575-24575
C	1220	-2.38	I6	56	LEMA-577.1.1	^{14}C-AMS	Charcoal	-	-	-	55.5	-24	-	21,401±95	25,925-25520
C	1222	-3.38	L6	64	ICA-16OS/0510	^{14}C-AMS	Sediment	-	-	-	*	-19.6	-	20,220±80	24,525-24045
C	1223	-2.9	L6-NW K6-NE	bear bone	Beta-345055	^{14}C-AMS	Bone (Extnd. Fig. 5e)	*Ursus americanus*	*	*	*	-12.1	*	27,830±150	31,975-31,220
C	1223	-3.4	L6-S	65	PRI-5414	^{14}C-AMS	Charcoal	*Pseudotsuga*	-	-	*	-22	-	27,929±82	31,920-31,355
C	1223	-2.95	J6-W	OSL 3A	Oxford X-7229	OSL	Sediment	-	-	-	-	-	-	23,940±2,950	N/A
C	1223	-2.9	L6-NW L7-SW	OSL 1 X11 (2012)	Oxford X-4135	OSL	Sediment	-	-	-	-	-	-	27,790±4,340 (minimum age)	N/A

% Collagen yield, percentage yield of extracted collagen as a function of the starting weight of bone samples. C:N, atomic weight ratio of carbon to nitrogen. %C is the percentage of carbon in the combusted sample. Stable isotope ratios of C and N are expressed in per mille (‰) relative to Vienna Pee Dee Belemnite and atmospheric N_2 (AIR). The calibrations were done using the OxCal 4.3 software[44] and the IntCal13 calibration curve[45]. *Missing chronometric data, owing to a lack in reporting or measurements on behalf of the laboratories. As per the Methods, strata for samples within SC-B were assigned following excavation and geological analysis.

Corresponding author(s): Ciprian F. Ardelean
cip_ardelean@hotmail.com;
aeci000206@uaz.edu.mx

Last updated by author(s): Apr 23, 2020

Reporting Summary

Nature Research wishes to improve the reproducibility of the work that we publish. This form provides structure for consistency and transparency in reporting. For further information on Nature Research policies, see Authors & Referees and the Editorial Policy Checklist.

Statistics

For all statistical analyses, confirm that the following items are present in the figure legend, table legend, main text, or Methods section.

n/a	Confirmed	
☐	☒	The exact sample size (*n*) for each experimental group/condition, given as a discrete number and unit of measurement
☐	☒	A statement on whether measurements were taken from distinct samples or whether the same sample was measured repeatedly
☐	☒	The statistical test(s) used AND whether they are one- or two-sided *Only common tests should be described solely by name; describe more complex techniques in the Methods section.*
☒	☐	A description of all covariates tested
☒	☐	A description of any assumptions or corrections, such as tests of normality and adjustment for multiple comparisons
☐	☒	A full description of the statistical parameters including central tendency (e.g. means) or other basic estimates (e.g. regression coefficient) AND variation (e.g. standard deviation) or associated estimates of uncertainty (e.g. confidence intervals)
☒	☐	For null hypothesis testing, the test statistic (e.g. *F*, *t*, *r*) with confidence intervals, effect sizes, degrees of freedom and *P* value noted *Give P values as exact values whenever suitable.*
☐	☒	For Bayesian analysis, information on the choice of priors and Markov chain Monte Carlo settings
☒	☐	For hierarchical and complex designs, identification of the appropriate level for tests and full reporting of outcomes
☒	☐	Estimates of effect sizes (e.g. Cohen's *d*, Pearson's *r*), indicating how they were calculated

Our web collection on statistics for biologists contains articles on many of the points above.

Software and code

Policy information about availability of computer code

Data collection	Data were collected by authors in Mexico (Universities of Zacatecas, Autónoma de San Luís Potosí, Nacional Autónoma de México, Instituto Nacional de Antropología e Historia INAH), United Kingdom (Universities of Oxford and Cambridge), Denmark (University of Copenhagen), U.S.A. (Kansas State University), and Brazil (University of São Paulo), using the softwares detailed below and institutional computers/databases, following the appropriate guidelines.
Data analysis	Genetic analysis involved Fastq-tools v0.8 for grepping poly A and T tails, SGA v0.10.15 for removing low complexity reads and duplicates, Bowtie2 v2.3.2 for database indexing and aligning reads against database, Samtools v1.10 for merging and sorting alignment files, ngsLCA - https://github.com/miwipe/ngsLCA for performing LCA on the alignment files, R v3.6.0, R studio v1.1.463 for parsing taxonomic profiles and figure production, MapDamage2.0 v2.0.8 for deamination estimates and read length distributions, Seqtk v1.2-r102 for generating fastq files from read IDs. Chronometric analysis involved OxCal v.4.3. Phytolith and pollen analysis involved Zen lite, C2 v.1.7.7. and TILIA/TILIAGRAPH v.2.0.41. OLS analysis involved the the Analyst v. 4.57 and R luminescence package v. 0.8.6. In-field finds were plotted using ArcMap v.10.3 and ArcScene v.10.3 (ESRI). Photogrammetry involved Adobe Photoshop CC19 v. 20.0.2 and Blender v.2.77. Figures were made using Adobe Photoshop CC19 v. 20.0.2. Further details on the methods and relevant code are included in the manuscript and the Supplementary Information.

For manuscripts utilizing custom algorithms or software that are central to the research but not yet described in published literature, software must be made available to editors/reviewers. We strongly encourage code deposition in a community repository (e.g. GitHub). See the Nature Research guidelines for submitting code & software for further information.

Data

Policy information about availability of data

All manuscripts must include a data availability statement. This statement should provide the following information, where applicable:

- Accession codes, unique identifiers, or web links for publicly available datasets
- A list of figures that have associated raw data
- A description of any restrictions on data availability

The data that support the findings of this study are available from the main text or Supplementary Information files. All sequence alignments are available from the European Nucleotide Archive under accession no. PRJEB37914.

Field-specific reporting

Please select the one below that is the best fit for your research. If you are not sure, read the appropriate sections before making your selection.

☐ Life sciences ☐ Behavioural & social sciences ☒ Ecological, evolutionary & environmental sciences

For a reference copy of the document with all sections, see nature.com/documents/nr-reporting-summary-flat.pdf

Ecological, evolutionary & environmental sciences study design

All studies must disclose on these points even when the disclosure is negative.

Study description	This is an archaeological study centred on the site of Chiquihuite Cave, and its cultural, palaeoenvironmental and geological findings.
Research sample	Lithic artefacts (N=1930), radiocarbon and OSL samples (N=46), eDNA sediment samples (N=31), pollen and phytolitch samples (N=9), chemical residue samples (N=3), micromorphology samples (N=1), petrography samples (N=12).
Sampling strategy	No statistical methods were used. Our sampling strategy was dependent on the available material within the excavation (number of lithic samples found, available locations for OSL and eDNA sampling, number of organic materials suitable for radiocarbon dating, etc).
Data collection	In the field, all archaeological finds were recorded at a station installed near the dig. Everything resembling an artefact was collected, avoiding on-spot subjectivity. Charcoals for AMS were immediately given separate codes. Every find bag received a number (1 to 2168). Each item got inventory numbers. Each find can be identified by the bag number plus inventory number, e.g., 206-13456. The final processing was done at the University of Zacatecas. If not laser-measured, the finds received 3D UTM coordinates based on provenience and depth, calculated manually, avoiding point overlap. This was carried out by the excavation director, C. Ardelean, and his students.
Timing and spatial scale	Data was collected between 2011 and 2018 in Mexico (Universities of Zacatecas, Autónoma de San Luís Potosí, Nacional Autónoma de México, United Kingdom (Universities of Oxford and Cambridge), Denmark (University of Copenhagen), U.S.A. (Kansas State University), and Brazil (University of São Paulo).
Data exclusions	No data were excluded. All results are duly reported.
Reproducibility	Multiple replicates, of subsamples from the same sample and multiple extracts, as well as replicated genomic libraries were performed and showed a remarkable similarity to samples from the same layers. Details of replication and results are described in the Supplementary Information. Sensitivity testing for Bayesian age modeling was carried out and described in the Supplementary Information.
Randomization	Our study was not experimental, therefore randomization does not apply.
Blinding	Our study was not experimental, therefore randomization does not apply.

Did the study involve field work? ☒ Yes ☐ No

Field work, collection and transport

Field conditions	Most information in this section has already been included in detail in the paper and in Methods. The field conditions were extreme. The excavation crew (only a few of the co-authors) spent 80 days in the field, in two separate seasons, living continuously inside the cave for up to 7 weeks in a row. The temperature inside the cave is stable at 12ºC in winter months. Light enters the cave only for two hours a day. The use of artificial light is mandatory and permanent. Due to extremely difficult conditions of work and the very remote location of the cave, which demands a 9 hrs climb from the nearest village, the crew must live at the cave for the entire duration of the season and also must involve the local community in the logistics. A new sampling trip has been specifically carried out fot the current resubmitted manuscript in order to obtain new samples and rerun the eDNA genetic studies.
Location	Chiquihuite Cave, Conception del Oro, Zacatecas, Mexico. Coordinates: 24.61666, -101.13333 (WGS84)

Access and import/export	All information is stated in the paper. The fieldwork, extraction of samples, as well as the export of samples (for dating, palaeobotanics studies and ancient eDNA analysis) were done with special and separate permites issued by the Mexico's Archaeology Council in Mexico City (see list below). The first author and several other co-authors work for Mexican institutions and have been following Mexican archaeological legislation since the inception of this research project. 1. Permits for the third and fourths field seasons (that include Chiquihuite's seasons of 2016-2017 and 2018-2019): a) Oficio 401.B(4)19.2015/36/2938 of December 21, 2015; b) Oficio 401.1S.3-2018/2224 of December 19, 2018. 2. Exportation permit for OSL tubes: 401-3-9554 of October 17, 2016. 3. Exportation permit for radiocarbon and eDNA samples: 401.3S.16-2017/1769&1770 of August 28, 2017. 4. Exportation permits for eDNA samples: 401.3S.16-2019/054 of January 15, 2019 & 676/2019-A-02, of January 29, 2019.
Disturbance	The disturbance has been minimal. The excavation spot followed a series of criteria meant to minimize impact on the cave structure and environment, as well as to the fauna, temperature and sound. We excavated in an area far from the entrance, inside the cave, near the northern wall where there is no risk of collapse from the roof, damage to the walls, danger for the crew or significant change in the cave's topography. We used a low-emission eco-friendly Honda generator, powered by gasoline, with very low noise and almost zero gas emissions. We did not obstruct the entrance to the cave, so the bats and birds could access it freely. No fireplaces were lit inside the cave. Cooking, fire, use of stove, biological needs, all was done outside in the forest in specifically desginated areas considering safety protocols and environmental protection.

Reporting for specific materials, systems and methods

We require information from authors about some types of materials, experimental systems and methods used in many studies. Here, indicate whether each material, system or method listed is relevant to your study. If you are not sure if a list item applies to your research, read the appropriate section before selecting a response.

Materials & experimental systems

n/a	Involved in the study
☒	☐ Antibodies
☒	☐ Eukaryotic cell lines
☐	☒ Palaeontology
☒	☐ Animals and other organisms
☒	☐ Human research participants
☒	☐ Clinical data

Methods

n/a	Involved in the study
☒	☐ ChIP-seq
☒	☐ Flow cytometry
☒	☐ MRI-based neuroimaging

Palaeontology

Specimen provenance	All specimens were excavated in excavation X-12, seasons 2016-2017, under the authorization issued by the Archaeology Council of the National Institute of Anthropology and History (INAH) in Mexico (see list of permits above). The study also involves ancient DNA obtained as environmental DNA directly from sediments in four stratigraphic layers (detailed in the paper). Same with the 9 sediment samples that served as basis for the pollen and phytolith studies (also detailed in the paper and SI).
Specimen deposition	Only fauna material can be referred to as specimens. The fauna specimens are currently in the possession of the Project crew at the University of Zacatecas, Mexico, in Zacatecas City. They will become freely available once the project has been terminated and the materials have been given to the national authority, the National Institute of Anthropology and History, according to the Mexican laws. Another part of the inventory is stored at the National Labs in Mexico City (INAH's Zooarchaeology laboratory). However, the specimens can be studied by other academics upon request. In the near future they will all be deposited at the INAH's national zooarchaeology lab and paaleontological repository, under the curatorship of Dr Joaquin Arroyo (co-author of this paper).
Dating methods	A few specimens have been dated by radiocarbon (AMS) and optically stimulated luminescence methods. Details of these are provided in the Supplementary Information.

☒ Tick this box to confirm that the raw and calibrated dates are available in the paper or in Supplementary Information.